Michigan State University

National Superconducting Cyclotron Laboratory

FISSION TIME SCALES FROM GIANT DIPOLE RESONANCES

PETER PAUL and MICHAEL THOENNESSEN

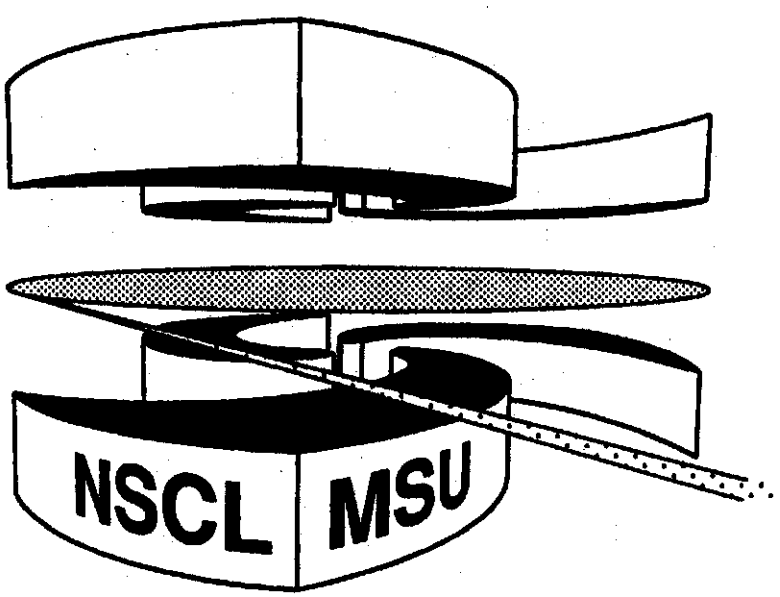

MSUCL-936

JUNE 1994

Michigan State University

National Superconducting Cyclotron Laboratory

UNIVERSITY AT STONY BROOK

STATE UNIVERSITY OF NEW YORK

FISSION TIME SCALES FROM GIANT DIPOLE RESONANCES

PETER PAUL and MICHAEL THOENNESSEN

MSUCL-936

JUNE 1994

To be published in Ann. Rev. Part. Nuc. Sci. 1994

FISSIONTIME SCALES FROM GIANTDIPOLE RESONANCES

Peter Paul

Department of Physics, Nuclear Structure Laboratory, State University of New York at Stony Brook, Stony Brook, New York 11794

Michael Thoennessen

Department of Physics and Astronomy and National Superconducting Cyclotron Laboratory, Michigan State University, East Lansing, Michigan 48824

KEY WORDS: hot nuclei, statistical model, fission dynamics, nuclear dissipation, nuclear viscosity, large amplitude collective motion

CONTENTS

1. INTRODUCTION

A major goal of contemporary nuclear physics is to understand the behavior of nuclear matter at finite and ,ultimately, high temperatures. Although the main focus is on temperatures of the liquid-gas phase transition and (eventually) the transition to the quark-gluon plasma, even modest heating of nuclei provides important new insights into fundamental nuclear matter properties. We define this regime as that below T $\sim$ 6 MeV, the limit to which an entire compound nucleus can be heated uniformly (1). One such fundamental property is the viscosity of nuclear matter and its evolution as a function of temperature. A basic example of the measurement of the transport properties of viscous nuclear matter is mass flow in the fission process. In this process a coherent mass motion is established inside the barrier and proceeds to fission either by tunneling through the barrier or at higher excitation energies through suitable transition states above the barrier. The time scale of this process is determined by the build-up of the fission flux inside the barrier, the flow across the barrier and the motion from the saddle to the scission point. The interior time scale can be estimated from the barrier assault frequency ω_1, with which the flux assaults the barrier $\tau_i = 2\pi/\omega \approx 20 \times 10^{-21}$s. The motion exterior to the barrier, i.e. from saddle to the scission point can be computed in the nonvicious liquid drop model to $\tau_o = 3 \times 10^{-21}$s (2). Any dissipation inside or outside the saddle lengthens these times. Thus one approach to the observation of nuclear viscosity is to measure the time scale of the fission process. Earlier studies of the fission process in the 1960s and 1970s used the kinetic energies of fission fragments as indicators of how much energy was lost from the collective process (3, 4).

Only since the early 1980s have major experimental refinements in particle and γ-ray analysis provided suitable clocks which have led to surprising new insights into the properties of nuclear dissipation. One clock suitable for measuring the time scale of the fission process comes from by the multiplicity of neutrons emitted prior to scission. This technique and its extensive results on dissipation in nuclear mass flow were summarized recently in a comprehensive review (5). A second clock is based on the emission of high-energy γ rays from the giant dipole resonance (GDR) excited in the hot fissioning compound nucleus prior to scission. This technique became available after it was realized in the mid-1980s that the GDR of a hot nucleus could be measured easily and after its properties were established systematically as a function of nuclear mass and temperature (6). The results on dissipation in the fission mass flow at temperatures up to $\sim$2 MeV obtained with this GDR clock

are the subject of this review.

Both techniques derived their driving power from the same initial surprise, obtained quite independently: In 1983, Gavron et al, Holub et al adn Hinde et al independently discovered that the neutron multiplicities (7- 9) at moderate temperatures were much higher than expected from the simple statistical model which rekindled interest in nuclear dissipation. In 1987, Thoennessen et al recognized that the GDR γ-ray multiplicities (10) in actinide nuclei between 40- and 80-MeV excitation energy were also much higher than expected. The rate at which the GDR emits γ rays would have had to be increased to several times the classical sum rule to explain the observed multiplicities unless the fission process was hindered significantly. These results are explained most directly and consistently by a large dissipation, which slows the fission process by more than an order of magnitude at temperatures between 1 and 2 MeV.

When fission time scales are studied using either of these two clocks, the hot compound nucleus is typically produced in a heavy-ion fusion reaction at an initial excitation energy E_{ex} from which a temperature can be derived by use of the level-density parameter a according to $E_{ex} = aT^2$. During the cooling process, as the nucleus moves toward scission, neutrons, charged particles, and γ rays are emitted in competition, in accordance with some statistical model (11). The cooling is interrupted when the fissioning nucleus reaches the scission point. Of course, the fission fragments themselves are left in an excited state and emit GDR γ rays or neutrons of their own. The fission fragment neutrons can be differentiated by their kinematics. In the case of γ rays the fission fragment contribution must be subtracted carefully from the total spectrum.

The GDR in the hot nucleus emits γ rays according to the strength function (12):

$$F(E_\gamma) = 2.09 \times 10^{-5} \frac{NZ}{A} \cdot S \cdot \frac{\Gamma_{GDR} E_\gamma^4}{(E_\gamma^2 - E_{GDR}^2)^2 + \Gamma_{GDR}^2 E_\gamma^2}. \qquad (1)$$

The GDR is useful as a clock because this strength function contains only three parameters: the sum-rule strength S ($S = 1$ corresponds to one classical sum rule), the GDR energy E_{GDR}, and the width Γ_{GDR}. In a deformed nucleus such as a fissioning system at or past the saddle, the GDR strength function is split into two components, resulting in a second width and the nuclear deformation as additional parameters (6).

Over the past decade these strength functions have been studied systematically for a wide range of nuclei and temperatures. The results, summarized in two complete reviews (6, 13), are as follows: (a) The GDR

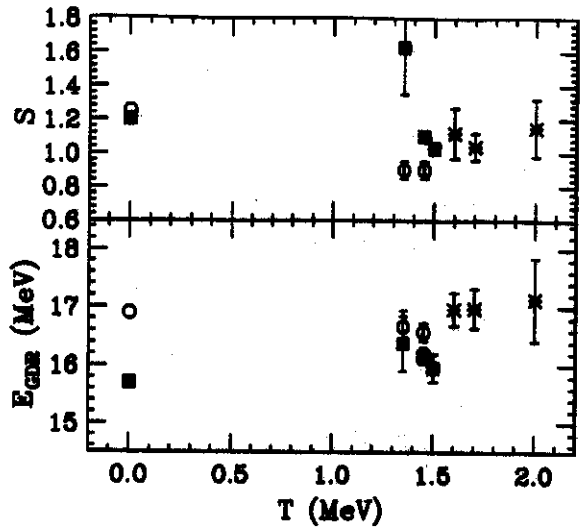

Figure 1: GDR energy E_{GDR} (bottom) and strength S (top) in units of one classical sum rule as a function of temperature for the mass region $A \sim 100$. Adapted from Ref. 14. Excited-state data for ^{92}Mo (o) and ^{100}Mo (■) and for ^{90}Zr and ^{92}Mo (×) from Ref. 15 are shown with ground-state values from Ref. 16.

energies are essentially unaffected by temperature (±3%) and can thus be taken from ground-state systematics. (b) The GDR width depends on nuclear excitation and angular momentum in a systematic fashion. (c) The GDR splitting due to nuclear deformation is well understood. (d) Most importantly, the intrinsic strength S is within ± 10% equal to one classical sum rule, independent of temperature over the range of nuclear temperatures discussed here. A sense of the uncertainty inherent in these basic assumptions can be gained from Figure 1, which shows the measured GDR energy and strength as a function of temperature (14) in the mass $A = 100$ region. The systematic behavior of the GDR parameter as a function of mass (13). has also been measured. The clock speed depends only on the strength function and the level-density parameter a, for which much systematic information as a function of nuclear mass and temperature is available (17, 18). Finally, the nuclear deformation can be determined simultaneously with the γ-ray multiplicity by measuring the γ-ray angular correlation relative to the spin axis of the fissioning system, which is perpendicular to the fission plane (19).

Thus the GDR clock has several advantageous features: (a) The simplicity of the GDR strength function and the absence of truly free parameters; (b) the fact that its rate does not depend on transmission factors; (c) the GDR vibrational time scale $\hbar\omega$ = 10 - 15 MeV, which is much faster than all fission time scales and thus ensures that the strength func-

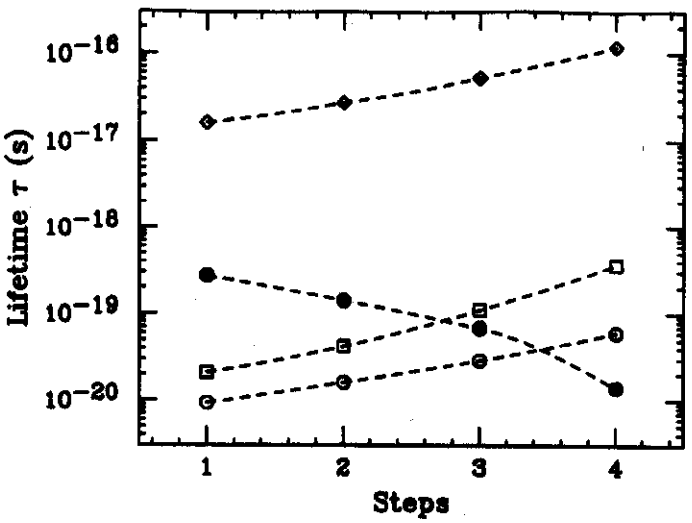

Figure 2: Compound nucleus decay times as a function of decay steps of the cooling process following the reaction ^{16}O + ^{208}Pb: γ-ray ($\diamond$), neutron ($\square$), unmodified fission (o) and dissipative fission ($\bullet$) lifetime. From Ref. 20.

tion follows the evolving deformation of the fissioning nucleus; and (d) the sensitivity of the GDR strength distribution and the γ-ray fission angular correlation to the deformation of the nucleus at the time of γ-ray emission.

Figure 2 gives a A sense for the intrinsic time scales of the GDR clock, the neutron clock, and the fission process. It shows these time scales in a hot ^{224}Th nucleus as it cools from its initial temperature of $\sim$ 1.6 MeV through the first four neutron decay steps, with and without dissipation (20). In the absence of dissipation, the fission process is faster than either the neutron or the GDR clock. However, in the presence of strong dissipation the neutron clock is initially faster but crosses the fission time scale as the nucleus cools past the third step.

2. FISSION TIME SCALES AND DISSIPATION

In this section we introduce the formalism that has been used to determine the fission time scales from the GDR γ-ray spectra and to translate these into a dissipation constant. We follow the approach of the Fokker-Planck equation (21, 22), which describes the evolution of the collective coordinates through phase space. It contains a dissipation coefficient $\eta = \beta m$ where β is the reduced dissipation coefficient, usually given in units of 10^{21} s^{-1}, and m is the inertial parameter of the motion. Alternatively, one can define η from the Einstein equation for the diffusion

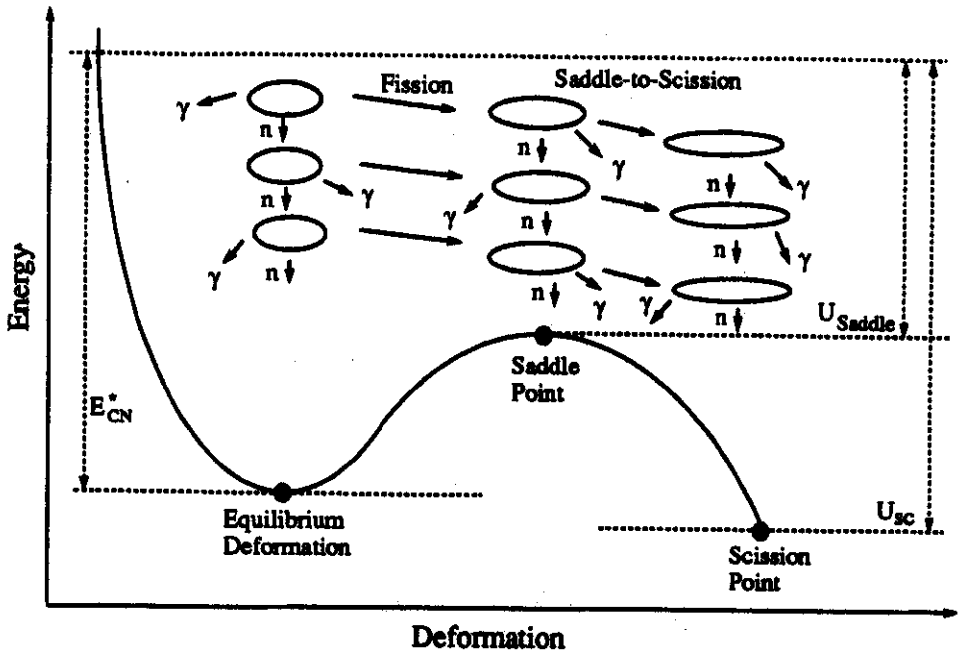

Figure 3: Schematic diagram of the cooling process as a function of deformation. Neutron- and γ-ray decay at the various stages together with the relevant energies is indicated.

constant $D = \eta T$ (23) It is useful to provide a natural scale to the dissipation by defining the nuclear friction coefficient $\gamma = \beta/2\omega$ (22, 24). This dimensionless constant describes the oscillation damping in the upright or inverted oscillator with frequency ω. Critical, overdamped and underdamped oscillations correspond to $\gamma = 1$, $\gamma > 1$ and $\gamma < 1$, respectively.

The presence of dissipation influences the fission process as well as particle and γ-ray emission in three regimes, as schematically depicted in Figure 3:

1. Inside the saddle: Starting from time $t = 0$, the fission flux builds up inside the barrier with a time constant τ_D. Thus the fission width at the saddle is given by (25, 26)

$$\Gamma_f(t) = \Gamma_f^0[1 - exp(-t/\tau_D)] \qquad (2)$$

The fission delay time τ_D allows for enhanced emission of particles and γ rays from inside the saddle. τ_D can be expressed in terms of the dissipation parameters β or γ. For the overdamped situation (which is the prevailing case) a useful approximation is given by (22, 27):

$$\tau_D = \frac{\beta}{2\omega_1^2} ln(10E_{Bar}/T) = \frac{\gamma_i}{\omega_1} ln(10E_{Bar}/T) \qquad (3)$$

where E_{Bar} is the fission barrier; ω_1 is the assault frequency; and γ_i is the normalized friction coefficient in the interior.

2. At the saddle: As the fission motion reaches the saddle, the viscous diffusion process results in a fission width that is reduced relative to the nonviscous width taken as the Bohr-Wheeler width Γ_f^{BW}, (28) as was recognized by Kramers (29):

$$\Gamma_f^{Kramers} = \Gamma_f^{BW}[\sqrt{1+\gamma^2} - \gamma]. \tag{4}$$

Here, $\gamma = \beta/2\omega_2$ contains the oscillation frequency ω_2 of the (inverted) barrier. Typically $\omega_1 \approx \omega_2$, and thus we take $\gamma \approx \gamma_i$. This approximation could be corrected in any specific case in which ω_1 and ω_2 are known. $\Gamma_f^{Kramers}$ then replaces Γ_f^0 in Equation 2. The reduction in fission width further enhances particle and γ-ray emission from the interior.

3. From saddle to scission point: The motion along this path is characterized by a time constant τ_{ssc}, which can be expressed in terms of the friction coefficient outside the barrier γ_o:

$$\tau_{ssc} = \tau_{ssc}^0[\sqrt{1+\gamma_o^2} + \gamma_o] \tag{5}$$

where $\tau_{ssc}^0 = 3 \times 10^{-21}$ s is the undamped time constant (2). The friction γ_o may be different from γ_i because γ_i contains the inertial parameter m, which depends on deformation (30), as well as the upright or inverted oscillator frequency ω.

Thus, when dissipation is introduced into the fission process it is described by just two parameters, γ_i and γ_o. This approach depends critically on the application of the Kramers factor to the fission width because it has the most dramatic effect. Figure 4 shows this drastic reduction of the fission width that results as γ_i is increased.

To put this graph in perspective, ground state fission has an upper limit $\gamma \leq 0.15$ (31); $\gamma > 0.2$ produces significant deviations from the statistical model; and $\gamma = 1$ is critical damping. We later show that this reduction of the fission width at high excitation energies is fully compatible with all observations at low energies.

3. EXPERIMENTAL METHODS

Determination of the fission time scales by using the GDR clock rests on the measurement of high-energy ($\sim 5 - 20$ MeV) γ rays in coincidence with fission fragments. Above ~ 2 MeV, the γ-ray spectrum is entirely

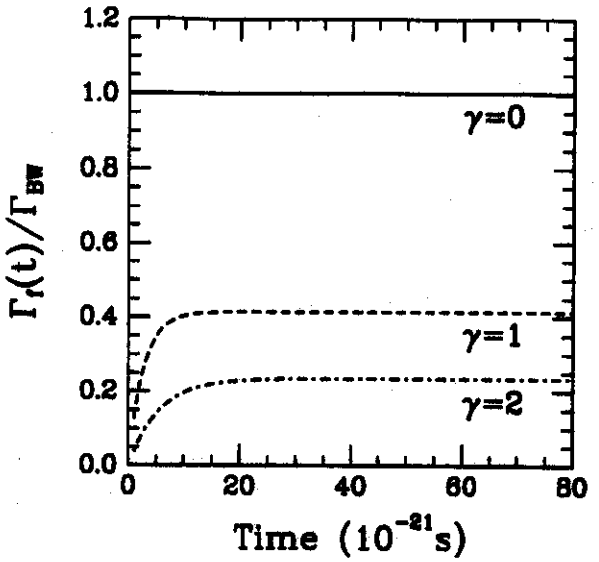

Figure 4: Evolution of the Bohr-Wheeler (solid line) and the Kramers fission decay widths for $\gamma = 1$ (dashed line) and $\gamma = 2$ (dotted/dashed line) as a function of time. The Kramers decay widths contain the transient effects of Equation 2.

dominated by GDR γ-rays, which stem from two sources: γ rays emitted from the GDR of the compound system prior to fission, including on the path from saddle to scission, and those emitted from the GDR from the highly excited fission fragments. These two sources contribute to different parts of the spectrum. Because of the smaller size of the fission fragments their GDR strength function peaks at a higher energy and, because the fission fragments cool down to the Yrast line, they dominate the low energy part of the spectrum ($\leq$ 8 MeV). The compound nucleus GDR is strong at intermediate energies, (8 – 12 MeV). The two contributions cannot be distinguished experimentally and must be calculated and subtracted carefully. A later example shows that this can be done with confidence. It is in principle not necessary to detect the fission fragments in coincidence in very fissile systems. However, because of the additional information provided by the γ-ray fission correlation, coincidence measurements are desirable. In the following sections we describe some experimental aspects of the γ-ray detection systems, the fission-fragment detectors, and the angular correlation measurements.

3.1 γ-Ray and Fission Measurements

A typical experimental set-up is sketched in Figure 5. It consists of one or several γ-ray detectors placed at 90^0 to the beam axis (for pur-

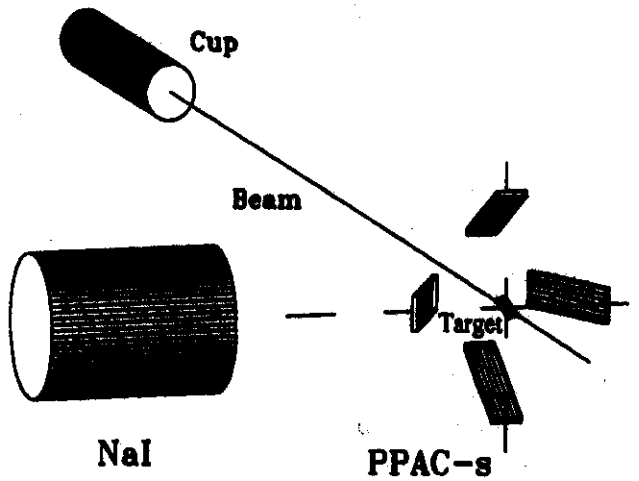

Figure 5: Experimental set-up for fission γ-ray coincidence measurements. Fission fragments are detected in four PPACs surrounding the targe, and the γ-rays are measured with a large-volume NaI(Tl) detector. From Ref. 32.

poses of the γ-ray - fission correlation) and four fission detectors, which detect fission fragments in kinematic coincidence such that the fission plane is defined both in-line and perpendicular to the γ-ray direction (19, 32). Most experiments use pulsed beams and time γ rays and fission fragments against the beam burst. This approach allows good neutron -γ-ray discrimination, and the time-of-flight (TOF) determination of the coincident fission fragments allows extraction of fission fragment masses and kinetic energies (32).

The first experiments that recorded γ-ray decay from the GDR built on highly excited states were performed with large-volume NaI(Tl) detectors surrounded by an active plastic anti-coincidence shield for cosmic ray suppression and improved resolution (6). The shape of the γ-ray spectra reflects the broad strength functions of the GDR. Even the deformation splitting is of the order of a few MeV. Thus the energy resolution of 2–3% achieved by large NaI crystals is usually adequate (6, 13). However, because the hot compound nucleus and fission fragments emit copious numbers of neutrons (three to five per reaction), the detectors must have an excellent neutron-γ-ray separation. If NaI(Tl) is used for time-of-flight discrimination the detectors must be at least $\sim$ 50 cm away from the target, because of the moderate ($\sim$ 1 ns) time resolution of NaI(Tl) crystals. Therefore, many recent experiments used either large-volume using BaF_2 detectors with shieldings similar to the NaI(Tl) detectors or closely packed arrays of hexagonal BaF_2 detectors. The en-

ergy resolution of BaF_2 crystals is worse ($\sim$ 5%) than that of NaI(Tl) (13). However, the superior time resolution ($\sim$ 400 psec) of BaF_2 (33) allows distances of $\sim$ 30 cm, which provides much larger solid angle coverage. In addition, BaF_2 crystals permit easy pulse-shape discrimination between γ rays, charged particles and energetic neutrons (34). The more or less exponential character of the γ-ray energy spectrum makes a good pile-up discrimination mandatory. Pile-up rejection is usually done by pulse-shape analysis (35), which for BaF_2 detectors is a means to distinguish neutrons from γ rays.

Because the γ spectrum lacks sharp features, reliable energy calibration and gain stability are crucial. The GDR energy range is typically bracketed by low energy γ-ray sources such as ^{228}Th (2.8 MeV) and PuBe (^{12}C, 4.4 MeV) and the high-energy decay γ rays from the 15.1-MeV state or the 22.3-MeV ground-state GDR in ^{12}C populated in a nuclear reaction. In hexagonal BaF_2 detectors one can also use the minimum ionizing peak from cosmic-ray muons (36), which deposit $\sim$ 40 MeV in a 6-cm horizontally positioned detector.

Comparison of the data with theoretical calculations requires knowledge of the detailed response function of the detectors as a function of γ-ray energy. These response functions can be obtained from nuclear reactions and then, for purposes of energy interpolation, simulated with Monte-Carlo computer codes like EGS (37) or GEANT (38). Instead of unfolding the response function from the data it is much more practical to fold the calculations with the energy-dependent response functions. All comparisons referred to in this review are based on this procedure.

The purpose of fission-fragment coincidence measurements is threefold: (a) to separate out events of inelastic scattering and fusion reactions leading to evaporation residues in reactions in which not all of the total cross section leads to fission, (b) to allow angular correlation measurements that provide information about the deformation of the γ-ray emitting system relative to the initial spin axis which produces a greater effect than would an angular distribution measurement relative to the beam axis, and (c) to determine the fission fragment mass distribution and total kinetic energy associated with a particular γ-ray decay event. The fission fragments are detected in parallel plate avalanche counters (PPACs), which determine angle and arrival time for each coincident fragment over a large solid angle. As long as binary decay can be assumed for the fusion-fission reaction, the masses and kinetic energies of both fission fragments can be obtained from a measurement of the time-of-flight and positions of coincident fragments. Figure 6 shows an example of the quality of the mass and energy information. Thus kinetic-energy and

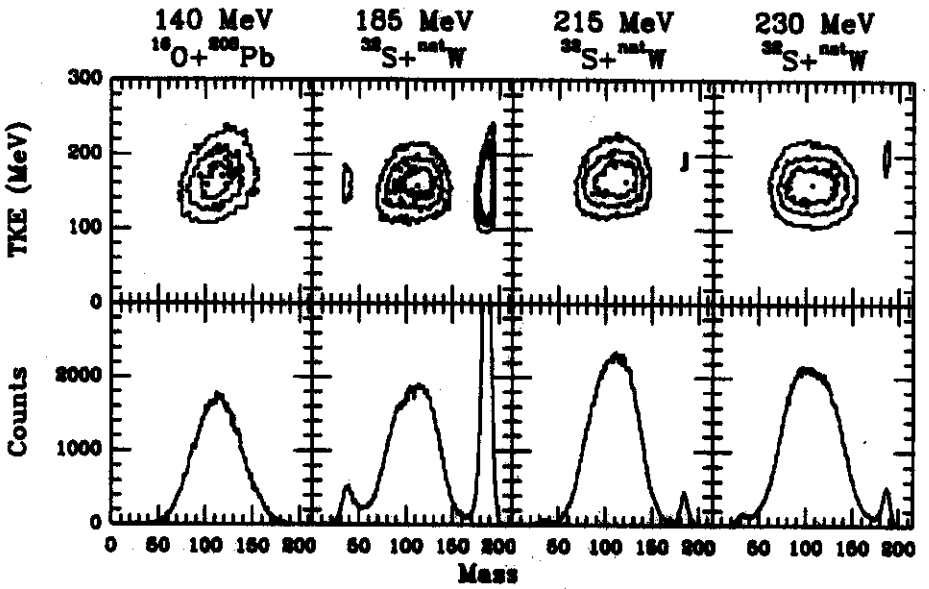

Figure 6: Mass and total kinetic energy distribution of fission fragments from the reactions ^{16}O + ^{208}Pb at 140 MeV and ^{32}S + ^{nat}W at 185, 215, and 230 MeV, in coincidence with GDR γ rays. From Ref. 32.

fission -mass cuts can be made event by event (32). The observed mass width of events associated with the hot GDR does not differ from the general sample. Unfortunately, this method does not provide absolute values for kinetic energies.

3.2 Fission γ-Ray Angular Correlations

The correlation of γ-ray emission relative to the spin axis, whose orientation is assumed to be oriented perpendicular to the fission plane, is a direct measurement of the deformation of the γ-ray emitting system and a very sensitive test for the presence of a long-lived deformed intermediate system as source of the γ rays. We present here a somewhat simplified explanation of Ref. 19.

The GDR resonance energy depends on the size and deformation of the nucleus. In a nucleus of ellipsoidal prolate shape, which is the most relevant case for fissioning nuclei, the GDR splits into vibrations along the major symmetry axis and perpendicularly along the (degenerate) minor axes. Thus the resonance develops a high energy component (perpendicular short axis) and a low energy component (parallel long axis). In this simple picture the high energy component has twice the sum rule

strength of the lower one. In a heavy-ion fusion-fission reaction, the reaction plane is defined by the beam axis and by the plane of the fission fragments. The initial axis of rotation is perpendicular to this plane. The spin axis is therefore always directed perpendicular to the symmetry axis of the prolate compound nucleus and parallel to one of the short principal axes. A dipole vibration along one of the principal axes emits radiation preferentially perpendicular to the vibration axis, which results in the angular distribution $W(\theta) = 1 + a_2 P_2(cos\theta)$, where θ is the angle between the spin axis and direction of γ-ray emission. In the high-spin limit and for collective rotating nuclei (where the axis of rotation is perpendicular to the symmetry axis) the coefficients for vibrations parallel and perpendicular to the symmetry axis are $a_2 = +1/2$ and $-1/4$, respectively. We note that in the γ-ray fission angular correlation, the spin axis is initially fixed in space. The selection of one spin axis gains a factor of two in sensitivity over angular distributions measured with respect to the beam axis, which average over all spin directions perpendicular to the beam. This averaging also changes the sign of the correlation.

This initial angular distribution must be corrected for the tilt of the fission fragments relative to the original spin axis on their way to the fission saddle. In accordance with traditional fission theory, this correction introduces a finite projection k of the spin onto the symmetry axis which is related to the tilt angle α by $cos^2\alpha = k^2/I(I+1)$. All averaging is over positive and negative tilts. With a statistical k distribution, the angular distribution for a given spin I is then

$$W_I(\theta) = 1 + a_2 P_2(cos\theta) - \frac{1}{2} a_2 (cos^2\theta - sin^2\theta) \frac{\sum_k \frac{3k^2}{I(I+1)} exp(-\frac{k^2}{2K_0^2})}{\sum_k exp(-\frac{k^2}{2K_0^2})} \quad (6)$$

where K_0 is the width of the normalized k distribution. The spin-averaged angular distribution is then obtained by summing over all spins populated in the fusion reaction weighted with their respective cross section.

The dependence on γ-ray energy is incorporated into the angular distribution by averaging over the GDR strength functions $F(E_\gamma)$ given in Equation 1:

$$W(\theta, E_\gamma) = \frac{\frac{1}{3} F_\parallel(E_\gamma) W_\parallel(\theta) + \frac{2}{3} F_\perp(E_\gamma) W_\perp(\theta)}{\frac{1}{3} F_\parallel(E_\gamma) + \frac{2}{3} F_\perp(E_\gamma)} \quad (7)$$

The factors of 1/3 and 2/3 come from the sum-rule splitting between the parallel symmetry axis and perpendicular axes.

A practical set-up contains two pairs of PPACs, one that defines defining the fission plane parallel to the γ-ray detector(s) axis, and one perpendicular to the γ-ray detector(s). The first pair measures γ rays emitted perpendicular ($\theta = 90^0$) to the spin axis, and the second pair measures γ rays emitted parallel ($\theta = 0^0$) to the spin axis. This arrangement is advantageous because the γ-ray detector can remain stationary, and data at 0° and 90° can be accumulated simultaneously. All efficiency uncertainties and beam-current fluctuations thus cancel out.

A convenient presentation of the anisotropy is a plot of the ratio $W(0°, E_\gamma)/W(90°, E_\gamma)$ as a function of γ-ray energy. The experimental ratio also contains the contributions from the fission fragments. When the predictions are compared with the data, these contributions must be included. Assuming nondeformed fission fragments, the ratio can then be written as:

$$\frac{W(0°, E_\gamma)}{W(90°, E_\gamma)} = \frac{\sigma_{pre}(E_\gamma)W_{pre}(0°, E_\gamma) + \sigma_{post}(E_\gamma)}{\sigma_{pre}(E_\gamma)W_{pre}(90°, E_\gamma) + \sigma^D_{post}(E_\gamma)} \tag{8}$$

where $\sigma_{pre}(E_\gamma)$ and $\sigma_{post}(E_\gamma)$ correspond to the calculated γ-ray energy spectra for pre- and postfission emission and $W_{pre}(E_\gamma)$ is the angular distribution derived in Equation 7.

The superscript D for the postfission γ-ray spectrum at 90° takes into account that these γ rays are Doppler shifted. Because it is not possible to determine from which fission fragment the γ ray was emitted, one must average over both directions of the velocity vector, toward and away from the γ-ray detector:

$$\sigma^D(E_\gamma) = \frac{1}{2}\left\{\sigma(E^+_\gamma)\frac{1}{1+\beta cos\alpha} + \sigma(E^-_\gamma)\frac{1}{1-\beta cos\alpha}\right\} \tag{9}$$

Here $E^\pm_\gamma = E_\gamma/(1 \pm \beta cos\alpha)$ is the Doppler-shifted γ-ray energy and, α corresponds to the angle between the fission fragment direction and the axis of the γ-ray detector.

4. THE STATISTICAL COOLING PROCESS

The highly excited compound nuclei needed to study fission at high temperatures are typically formed in heavy-ion fusion reactions. The deexcitation, or cooling, of these compound nuclei is described in the framework

of the statistical model. It is based on the assumption that all nuclear degrees of freedom are equilibrated after the formation of the compound nucleus and before it begins to decay. Several computer codes [CASCADE (39), PACE2 (40), ALERT1 (41), HIVAP (42), etc.] model the statistical decay. The details are described in the references for the codes. In this section we concentrate on the modifications necessary to describe the pre- and postscission γ-ray components of the measured γ-ray spectrum in a heavy-ion fusion-fission reaction. In particular, we discuss the incorporation of dissipation, the simulation of the particle and γ-ray decay during the descent from saddle to scission as well as in quasifission reactions, and the calculation of the decay of the highly excited fission fragments.

4.1 The Compound Nucleus

In a heavy-ion fusion reaction, the compound nucleus is formed at a specific excitation energy and with a spin distribution given by the measured fusion cross section and the sharp cut-off model. Thus one can calculate a maximum spin of the compound nucleus. Larger spin values lead to quasifission and deep inelastic scattering. The relative decay rate of a given state (i) to a set of final states (f) is purely given by the level densities of the final states and the transmission coefficient of the emitted particles. In the case of γ-ray emission the transmission coefficients is replaced by the photo-absorption cross section inverted by use of the reciprocity theorem (12):

$$R_\gamma = \frac{\rho_1(E_f, J_f)}{h\rho_1(E_i, J_i)} F(E_\gamma) \tag{10}$$

where $F(E_\gamma)$ is the GDR strength function from Equation 1 and ρ_1 is the level density at the equilibrium deformation.

The fission decay rate is included with help of the transition-state model by integrating over all available states at the saddle point (3):

$$R_f = \frac{1}{h\rho_1(E_i, J_i)} \int_0^{E_i - E_f} \rho_2(E_i - E_f - E_s, J_i) dE_s \tag{11}$$

where $E_f = E_{rot}(J_i) + E_{bar}(J_i)$; E_{rot} is the rotational energy; E_{bar} is the fission barrier; and ρ_2 is the level density at the barrier. In principle, these two densities (ρ_1 and ρ_2) can contain different level density parameters and if the density at the barrier is reduced artificially, it can mimic the effect of dissipation. However, all evidence (and one's physical intuition)

indicates that, if anything, the level density is enhanced at the barrier as a consequence of increased deformation. All recent analyses use the same value in ρ_1 and ρ_2.

An important parameter is the spin dependent fission barrier $E_{bar}(J_i)$. The parameterization of Sierk, which is based on the liquid drop model and includes finite range effects, (43) is widely used. Recently, the temperature dependence of these fission barriers wasincluded in the statistical model calculation (44).

Because the fission decay width is a calculated parameter within CASCADE, the Kramers modification is easily incorporated by modifying this width according to Equation 2. However, the time dependence of Equation 2 is not straightforward because statistical model codes are based on decay steps and do not follow the time evolution of the system explicitly. The time dependence of the fission probability build-up inside the saddle can be included by changing it according to Equation 2 with the elapsed time appropriate for each step. The fission decay width of the statistical model differs from the fission decay width of the transition-state model by a factor of $\hbar\omega_1/T$ (22, 45). Thus the present formalism relies on the approximation $\hbar\omega_1/T \approx 1$, which is commonly applied (24, 26, 46- 48). The exact dependence of this ratio, especially as a function of spin, and the effect on the extracted dissipation parameter have not been studied.

Integrating the γ-ray yield over all decay steps produces the γ-ray spectrum emitted from the compound nucleus. If 100% of the fusion cross section leads to fission, the result is equivalent to the "presaddle" contribution to the total γ-ray spectrum. If a fraction of the fusion cross section leads to evaporation residues, one must use Monte-Carlo calculations to extract those γ rays of the decay chains that eventually fission. Alternatively, the following much faster subtraction method can be applied (26). First, one calculates the relative residue and fission cross section probabilities as a function of spin. nexta γ-ray spectrum is obtained from a separate CASCADE calculation using the residue-connected spin distribution as the starting distribution and fission artificially "switched off." This yield is identified with the γ-ray spectrum of decay paths leading to evaporation residues. Subtracting it from the original calculation yields the prefission γ-ray spectrum.

4.2 The Saddle-to-Scission Path

After the fissioning system crosses the saddle, especially in highly fissile systems where the saddle point has a very compact shape, particles and GDR γ-rays may be emitted during the descent from the saddle point

to scission. The deformation dependence of the GDR strength function results in different spectral shapes depending whether the γ rays are emitted outside or inside the saddle point.

A few assumptions are necessary to calculate γ-ray and particle emission between saddle and scission. Although the system certainly is not equilibrated in all nuclear degrees of freedom, one can apply the statistical model within small time steps, calculate the decay probabilities during this time and then adjust the time-dependent parameters for calculation of the next step. The most important time dependent parameters are the deformation, which increases toward scission and increases the splitting of the GDR energies, and the excitation energy, which increases from the saddle point energy (26)

$$U_{saddle} = E_{ex} - E_{Bar} - E_{rot}(saddle) \tag{12}$$

to the scission-point energy

$$U_{sc} = E_{ex} + Q_f - TKE - E_{rot}(scission) - E_{def} \tag{13}$$

where Q_f is the Q-value for fission, TKE is the total kinetic energy of the fission fragments; and E_{def} is the deformation energy bound in fragment deformation. At high excitation energies, average values are adequate for those quantities.

In contrast to the compound nucleus decay, the saddle-to-scission motion has a fixed time constant τ_{ssc} influenced only by dissipation. The γ-ray or particle emission is restricted to this time. The statistical code calculates the time elapsed for each consecutive decay step and stops when τ_{ssc} is reached.

In the fusion of more symmetric reaction partners, a fraction of the fusion cross section may populate spins of the compound nucleus for which the fission barrier has vanished. In such cases, no real compound nucleus is formed, and the nucleus moves directly on a path toward scission. Particle and γ-ray emission on this path can be treated similarly to the saddle-to-scission decay.

Figure 7 gives an example of the quality of these procedures. It shows the γ-ray spectrum (top panel) observed in coincidence with fission fragments obtained in the reaction of 140 MeV ^{16}O on ^{208}Pb and the γ-ray - fission angular correlation (bottom panel). The reaction produces ^{224}Th at an initial excitation energy E_{ex} = 82 MeV (32). The spectrum displays the characteristic giant-resonance shelf between 8 and 15 MeV, but the entire spectrum, down to 5 MeV, results from γ-ray emission from GDR strength functions. The computed contributions of the presaddle

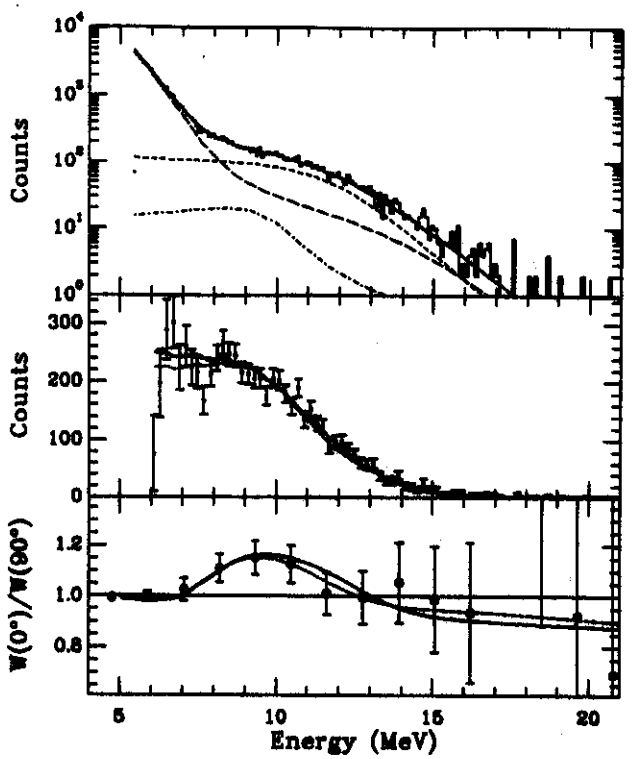

Figure 7: Total γ-ray spectrum (top), prefission contribution (center) and fission-γ-ray angular correlation (bottom) following the reaction $^{16}O + ^{208}Pb$ compared with a statistical model calculation as described in the text. The total γ-ray spectrum (solid line) in the top panel consists of γ-ray contributions from prescission (short-dashed line), saddle-to-scission (dotted/dashed line), and postscission emission (long-dashed line). From Ref. 32.

emission, of the saddle-to-scission emission from the compound nucleus, and of the fission fragments (see next section for more details) are indicated separately and combine to achieve an excellent fit over the entire spectrum. The fission fragment γ rays dominate at low and high energies (where the GDR from the hot but smaller fission fragments is centered). After the calculated contributions from the fission fragments are subtracted from the experimental spectrum, a clean GDR contribution from the compound nucleus remains (center panel). This strength peaks just at the γ-ray energies where the γ-ray fission angular correlation (bottom panel) indicates γ-ray emission from a deformed long-lived intermediate system, i.e. the compound nucleus.

The peak corresponds to the component of the GDR shifted downward in energy by the deformation, i.e. the vibration along the long axis. The up-shifted component corresponding to the vibration along a short axis is overshadowed by the strong GDR of the fission fragments.

Table 1: Compound nucleus GDR energies (E_1, E_2), widths (Γ_1, Γ_2), and strength (S_1, S_2), of the two components used in the statistical model calculation for prolate and oblate shapes of ^{224}Th at E_{ex}=82 MeV in the ^{16}O + ^{208}Pb reaction. All energies in MeV.

Deformation	E_1	Γ_1	S_1	E_2	Γ_2	S_2
$\beta = 0.3$, coll. prolate	11.0	4.2	1/3	14.0	5.8	2/3
$\beta = -0.1$, non-coll. oblate	12.1	5.5	2/3	13.3	6.5	1/3

The statistical model results in an excellent fit to the compound GDR spectrum and the γ-ray fission angular correlation, using the standard GDR parameter set given in Table 1. The correlation agrees with either a prolate deformation (Figure 7, center and bottom panels, solid lines) similar to that of the thorium ground state or a noncollective deformation (dashed lines) predicted by the rotating liquid drop model for the average angular momentum of the compound system. Only the friction constant γ_i is a fully free parameter. This fit requires a large friction constant $\gamma_i = 10$ to reproduce the large GDR contribution from the compound nucleus.

At higher bombarding energies and for reactions using heavier projectiles such as ^{32}S, quasifission becomes important for high angular momenta (49, 50). The procedures outlined above can be applied to calculate the γ-ray and particle emission during the quasifission process (26, 32).

In this process the two colliding nuclei initially face a (conditional) saddle where the system is not fully equilibrated because of the strong neck formation. The conditional saddle is higher than the fully equilibrated (unconditional) saddle and the system needs additional energy (extra push) to pass this saddle.

After crossing the conditional saddle, the system equilibrates rapidly in all degrees of freedom except shape. Because of the dissipative losses incurred during this stage, the system fails to pass the unconditional inner saddle and moves toward reseparation unless a compensating energy increment (extra-extra push) is available. Figure 8 outlines the angular momentum region for which this process is important for the reaction ^{32}S + W $\rightarrow$ Th at three bombarding energies. For a fixed bombarding energy, all partial waves to the left of the extra-push energy line (E_x) overcome the conditional saddle, but only those to the left of the extra-extra push line (E_{xx}) form a compound nucleus. The others undergo

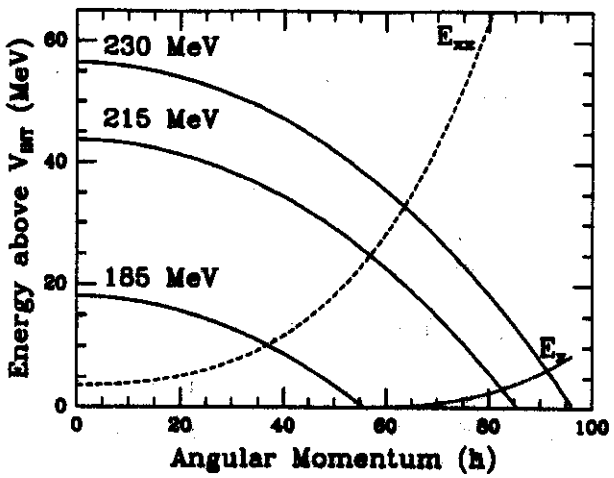

Figure 8: Extra- and extra-extra push energies and the energy above the interaction barrier V_{INT} for the reaction $^{32}S + ^{184}W$ at 185 MeV, 215 MeV, and 230 MeV. From Ref.32.

quasifission which proceeds much more rapidly than compound fission (49, 52).

Nevertheless, the system may emit γ rays and particles, which can be calculated in a manner similar to that used for saddle-to-scission decay. The initial excitation energy of the system can be estimated from the ion-ion potential after the conditional saddle and the final energy is the excitation energy at the scission configuration. In all other respects, γ-ray emission is treated like the saddle-to-scission path (26).

4.3 Cooling of the Fission Fragments

After scission, the fission fragments are repelled from each other by the Coulomb force, which produces a total kinetic energy independent of the initial compound nucleus excitation energy. Thus the excitation energy of the fission fragments is proportional to the compound nucleus excitation energy. The emission of particles and γ rays from the highly excited fission fragments can be calculated using the statistical model procedures discussed above.

Standard statistical-model codes, which include the fission channel, do not follow the subsequent decay of the fragments. Thus modifications are necessary to keep track of the available excitation energy and spin at scission and to calculate the other important initial conditions for the decay of the fragments (19). The total fission cross section is distributed over a wide range of masses, the width of which is given by

experiments. The corresponding Z of the primary fission fragments can be derived, assuming equal charge displacement (3): $(Z_f - Z_{stable})_{light} = (Z_f - Z_{stable})_{heavy}$. Thus the differences between the most probable Z of the fragment (Z_f) and the Z of the most stable isobar (Z_{stable}) are the same for light and heavy fission fragments. The most stable isobars follow the valley of stability and can be calculated with Green's formula (53): $N - Z_{stable} = 0.4A_f^2/(200 + A_{ff})$. The initial excitation energy of the fragments is proportional to their mass:

$$E_{ex}^{ff} = A_{ff}/A_{fiss}(E_{ex}^{fiss} + Q_f - TKE). \quad (14)$$

The subscripts ff and $fiss$ correspond to the fission fragments and fissioning nucleus, respectively. Q_f is the Q value for fission for the specific nuclei and the total kinetic energy (TKE) has a Gaussian distribution derived from the Viola systematics (54). The total available spin J_T of the fission fragments can be taken from a parameterization of measured γ-ray multiplicities of the fission fragments: $J_T = 2/7J_{Fiss}+18.0-0.17J_{fiss}$ (19, 55). It is assumed that the total spin J_T is distributed equally between the two fragments: $J_f = J_T/2$.

In practice, the initial fission cross section as a function of E_{ex}^{Fiss} and J_{Fiss} is distributed over a four-dimensional array consisting of A_{ff}, Z_{ff}, E_{ex}^{ff}, J_{ff}, and subsequent CASCADE calculations are performed for each individual nucleus A_{ff}, Z_{ff}, which results in hundreds of individual calculations. The γ-ray spectra of these calculations added together yield the postfission γ-ray spectrum.

This procedure is based on many assumptions, parameterizations, and approximations, and it is important to verify the results of these calculations. This is done most effectively by computing the γ-ray and particle spectra observed in spontaneous fission, in which no GDR γ rays are emitted prior to scission. The only case measured to date is the spontaneous fission of ^{252}Cf (56- 61). Interestingly, the GDR built on highly excited states was first observed in this nucleus, but its significance was not realized at the time (56).

Figure 9 shows the experimental γ-ray data from several experiments that reach $\sim$ 20 MeV, i.e. beyond the GDR peak energy of the fragments. The data are described by a statistical model calculation in which all parameters were taken from other experiments and none fitted to the spectrum. An excellent absolute prediction of the γ-ray multiplicity is achieved over the entire spectrum. The γ rays above 10 MeV come from the first step after the fission fragments separate. If at this early time after scission 40%, or 7 MeV, of the available excitation energy is still bound up in collective modes, the high-energy part of the spectrum is

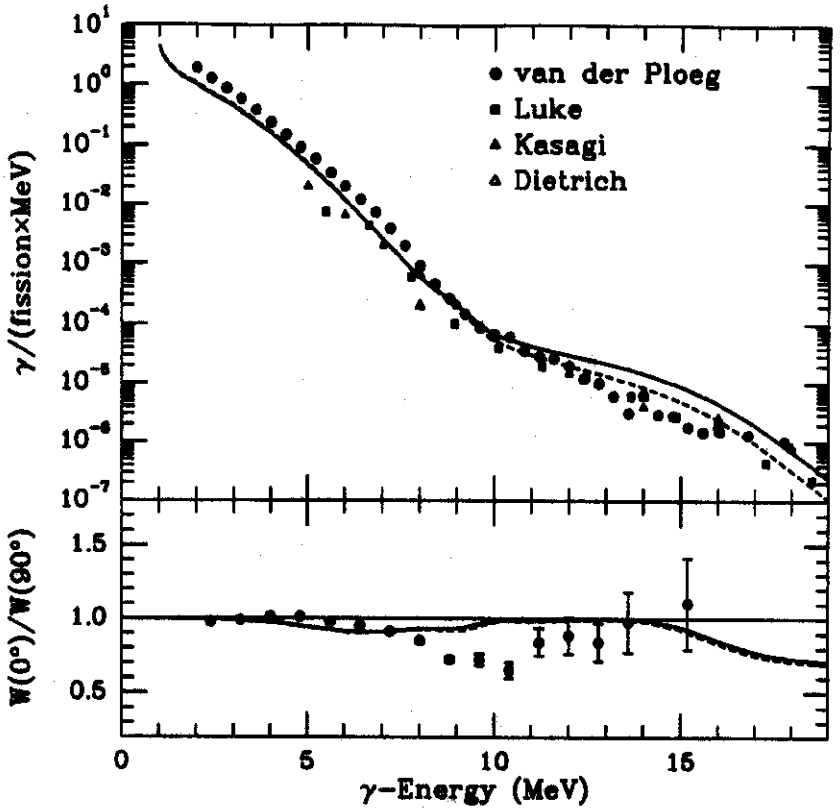

Figure 9: Several measurements of the γ-ray spectrum following the spontaneous fission of ^{252}Cf, compared with a statistical model calculations as described in the text. The angular distribution data are from Ref. 60. From Ref. 62.

reduced, as shown by the dashed line in the figure. However, the large reported γ-ray - fission anisotropy, which simply cannot be understood within our model, strongly contradicts this observation. Extensive neutron data are also available for this nucleus, and the same parametrization explains these data in considerable detail (62).

The successful description of the fission-fragment cooling in ground-state fission without any fitted parameter gives confidence in the subtraction procedure used in hot nuclei.

5. EXPERIMENTAL RESULTS

This section presents examples of the data and their analyses that provide the core evidence for large dissipation inside and outside the saddle by use of the GDR clock. We restrict ourselves to compound nuclei in the actinide region, where the fission channel dominates at all bombarding

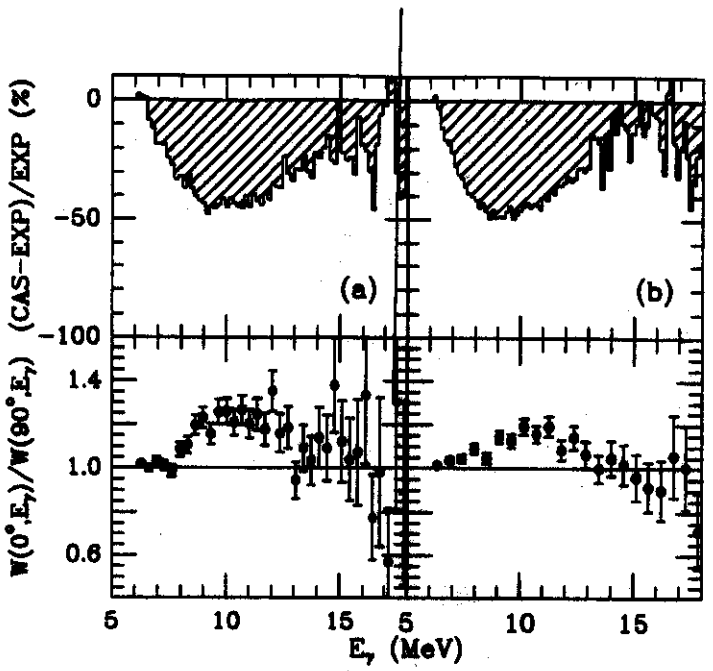

Figure 10: Difference spectrum (top) and angular distribution (bottom) for the reaction ^{16}O + ^{208}Pb at 120 MeV (a) and 140 MeV (b). From Ref. 26.

energies and for which the most systematic results are available. A few lighter nuclei that were studied, such as ^{200}Pb and even lighter ones, yielded similar results.

5.1 Dissipation Inside the Saddle

The compound nuclear system studied first and most extensively is thorium. Figure 7 shows the γ-ray spectrum and γ-ray - fission angular correlation obtained in the reaction ^{16}O + ^{208}Pb at 140-MeV bombarding energy which produces ^{224}Th at an initial excitation of 90 MeV, equivalent to a temperature T = 1.9 MeV. The excellent fits in this figure require a very large dissipation constant $\gamma = 10$.

It is instructive to demonstrate the serious discrepancy between the measured γ-ray multiplicity and a nondissipative statistical model. Figure 10 shows the difference of predicted yield minus observed yield on a linear scale for two bombarding energies. In each case the experiment shows twice the number of γ rays that is predicted by the nondissipative model exactly in the energy region where the angular correlation indicates the γ rays from the GDR of the deformed compound system. To fit the γ-ray spectrum in this energy region one would have to speed up the GDR clock to four times the classical sum rule – a serious violation of basic nuclear physics – or slow down the fission process in the hot

compound system by strong dissipation (26).

The sensitivity of the spectral fits to the dissipation parameter can be seen in Figure 11. Here, the same data set is fitted with identical GDR and level-density parameters but with a dissipation constant increasing from a very underdamped case ($\gamma = 0.1$) through critical damping ($\gamma = 1$) to a strongly overcritical damping ($\gamma = 10$). Only this large dissipation constant value corresponding to strongly overcritical damping fits the γ-ray spectrum. Both the spectrum and the γ-ray - fission angular correlation are sensitive to the nuclear deformation and thus the dissipation. Although no additional fitting was done for the description of the correlation, agreement with the γ-ray fission angular correlations is noticeably improved as γ increases. Without any additional parameters the same calculations also yield simultaneously the neutron multiplicity. Again, only $\gamma = 10$ reproduces simultaneously the observed neutron multiplicity (see Section 6.1).

This strong dissipation slows the fission process significantly (26) from 4.2×10^{-20} s ($\gamma = 0$) to 6.4×10^{-19} s (averaged over the various decay steps). At first sight this slowing appears to affect the overall fission probability and thus to conflict with existing data. However, this is not the case. The bulk of the fission probability simply is shifted to later steps of the decay cascade after the nucleus has cooled. At these stages close to the ground state fission is underdamped (31), and the system fissions according to the full Bohr-Wheeler decay width. This process ensures that the total fission probability is conserved (see Section 6.2).

The same dissipation constant ($\gamma = 10$) was extracted in several other systems, e.g. in the reaction $^{16}O + ^{159}Tb$ leading to ^{175}Ta at $E^* = 123.4$ MeV (63) and $^{32}S + ^{nat}W \rightarrow ^{\sim 216}Th$ (32).

A critical parameter in all statistical model calculations is the nuclear level density. One must consider whether a change in the parameter a with increasing temperature could explain the data without resorting to dissipation. The temperature dependence of the level density has been studied extensively (18, 64). For a nucleus of $A = 210$, the inverse level-density parameter $k = A/a$ increases from 8.8 at $T = 0$ MeV to ~ 10 at $T = 2$ MeV. In the case at hand, ^{232}Th, the average temperature is 1.4 MeV which results in $k = 9.2$. The above analyses used $k = 9 \pm 0.2$ for the compound system and somewhat higher values for the fission fragments (10) consistent with the theoretical predictions.

The detailed model description behind the calculation of the γ-ray multiplicity allows us to differentiate between γ rays emitted from inside the barrier (presaddle) and those emitted from the saddle-to-scission path. As shown in Figure 11 ($\gamma = 10$), the excess prefission GDR γ rays

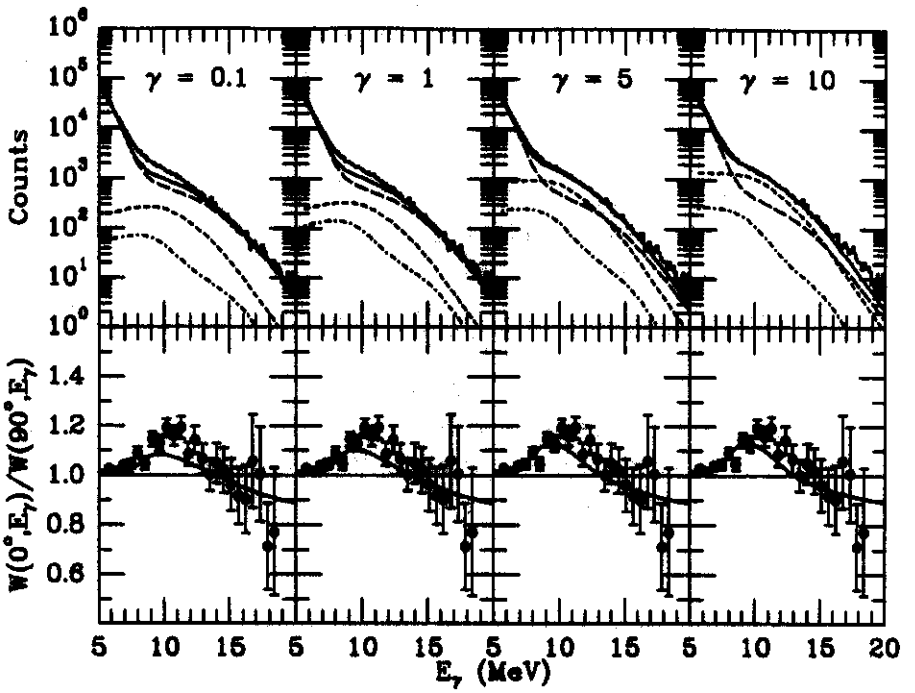

Figure 11: Comparison of statistical model calculations with different dissipation coefficients for the measured γ-ray spectra and the angular distribution for the reaction $^{16}O + ^{208}Pb$ at 140 MeV. The individual contributions to the total calculated γ-ray spectrum are the same as in Figure 7. From Ref. 26.

in ^{224}Th stem overwhelmingly from inside the barrier. When these calculations are extended to heavier nuclei, the results compiled in Figure 12 demonstrate that in heavier systems the presaddle contribution decreases whereas the emission from the saddle-to-scission path becomes increasingly important.

5.2 Dissipation from Saddle to Scission

The dissipation constant depends on an inertial mass parameter and on the nuclear shape. The constant for the saddle-to-scission motion γ_o may well be different from the dissipation constant inside the saddle γ_i, which was in effect determined in the previous section. γ_o can be determined in heavier systems, in which the pre-fission γ-ray spectrum is dominated by the saddle-to-scission contribution (as exemplified in Figure 12).

This approach has been applied using the reaction $^{32}S + ^{208}Pb$, which leads to the compound nucleus ^{240}Cf at $E_{ex} = 93$ MeV. Although the saddle-to-scission GDR γ rays do not yet dominate the prefission contribution in this mass region, one can extract γ_o by keeping γ_i constant at

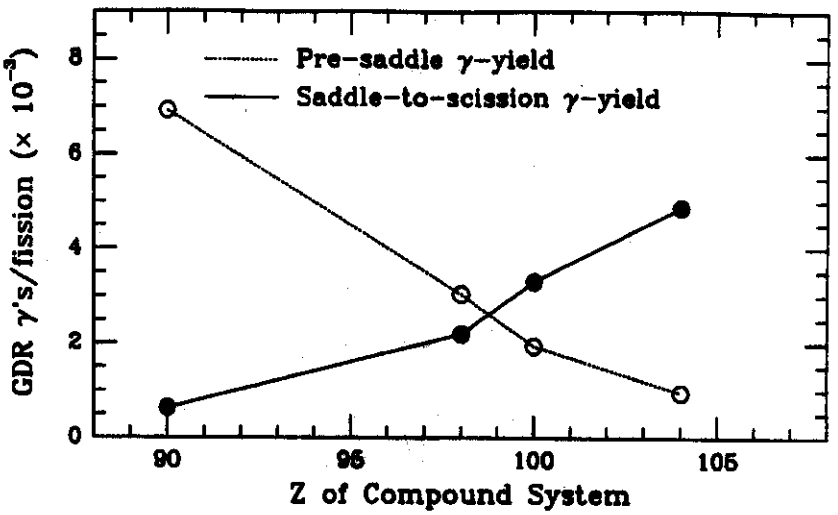

Figure 12: Calculated GDR γ-ray probability for presaddle (o) and saddle-to-scission (•) emission as a function of compound nucleus. From Ref. 65.

the value extracted from ^{232}Th. This conclusion is based on the assumption that the global parameters of mass flow at higher energies (where shell corrections should be unimportant) do not change much from one nucleus to the next.

Figure 13 depicts the γ-ray spectrum and the γ-ray fission angular correlation for this reaction and includes the statistical model fits. The individual contributions to the γ-ray spectrum are the same as in Figure 7. In the fits, γ_i was kept at 10, and the saddle-to-scission time τ_{ssc} (which depends on γ_o) was varied as the fit parameter for the dissipation outside the saddle. The best fit yields (quite sharply) $\tau_{ssc} = 26 \times 10^{-21}$ s. With the help of Equation 5 this result translates into $\gamma_o = 4.3$. τ_{ssc} is quite insensitive to the dissipation constant inside the saddle. If γ_i is reduced to 5, the best-fit τ_{ssc} increases only to 30×10^{-21} s and γ_o increases to 5.0 (65). The dissipation constant outside the saddle is also not very sensitive to the level-density parameter; when a is varied from $A/8.8$ to $A/10.0$, γ_o changes from 4.3 to 2.4. Thus γ_o appears to be noticeably smaller than γ_i. Its value corresponds to the full one-body surface-plus-window dissipation and is much larger than the effect deduced from mean total kinetic energies of the fission fragments at lower energies (66). However, it is in line with recent dynamical calculations of neutron multiplicities and fragment kinetic energies (67).

A recent experiment extended these measurements to a heavier system in the reaction (^{28}Si + ^{208}Pb $\rightarrow$ ^{260}Rf). In this nucleus, the contribution from inside the saddle should be vanishingly small. However, in this

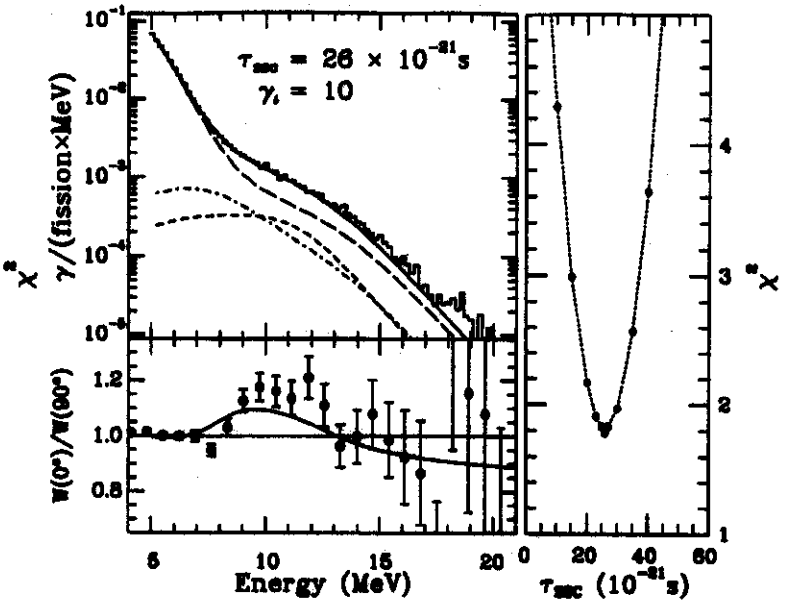

Figure 13: γ-ray spectrum and angular correlation for the reaction ^{32}S + ^{208}Pb at 230 MeV (left). The right panel shows the χ^2 for γ-ray energies between 8 and 25 MeV as a function of the fit parameter τ_{ssc}. From Ref. 65.

case the sensitivity to the compound system is already much reduced by the increasing strength of γ rays originating from the fission fragments, which have very high excitation energies (68).

Another experiment forming an even heavier compound system at a high excitation energy provided evidence of an excess of prefission GDR γ-ray yield (69). Figure 14 shows the total γ-ray spectrum in coincidence with symmetric fission fragments following the reaction of 272 MeV ^{40}Ar + ^{232}Th leading to ^{272}108 at an initial excitation energy of ~105 MeV (left) and ~240 MeV (right). The excitation energy of the fragments should be 90 MeV and 140 MeV, respectively. Although no detailed statistical model calculations comparable to the previous examples were performed, simple approximations indicated the presence of prefission γ rays.

The left side of Figure 14 shows that fission-fragment excitation energies of 100 MeV (dotted line) which would be expected from the normal nondissipative energetics, predict too large a yield of fission-fragment γ-rays. A reduction of the fission-fragment excitation energy to 60 MeV (solid) — which corresponds to a cooling of the compound nucleus before fission — is necessary to describe the data.

At the larger excitation energy (Figure 14, right), a reduction from

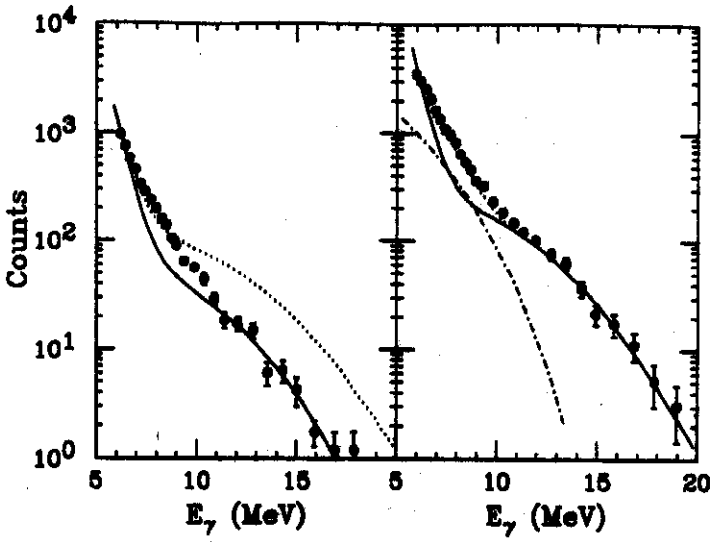

Figure 14: γ-ray spectra in coincidence with symmetric fission fragments following the reaction ^{40}Ar + ^{232}Th $\rightarrow$ ^{272}108 at E_{lab} = 272 MeV (left) and E_{lab} = 420 MeV (right). The left curve shows calculations for fission fragments at E_{ex} = 60 MeV (solid line) and E_{ex} = 100 MeV (dotted line). The right panel shows a calculation for the total γ-ray spectrum (dotted line) consisting of the sum of the fission fragments (E_{ex} = 80 MeV, solid line) and prefission (dotted/dashed line) contribution. Adapted from Ref. 69.

140 to 80 MeV (solid line) is required. This panel also shows a calculation for the prefission γ rays (dot-dashed line) expected from the GDR of the A = 272 nucleus that fills in the discrepancy in the γ-ray spectrum between 6 and 10 MeV. The GDR position was taken as 11 MeV, in line with ground-state systematics for spherical systems. A large deformation, as one might expect in this case, would move the GDR position to an even lower energy. Based on the predictions in Ref. 18, the temperature of this very heavy system does not increase much with excitation energy because the level-density parameter is increasing rapidly.

5.3 Energy Dependence of Dissipation

A major argument against these very large dissipation constants is that they would contradict the long set of data on fission probabilities and fusion evaporation cross sections that exist at low excitation energies. Thus it was clear early in the course of these studies that the dissipation constant must have some dependence on temperature so that the fission process regains its normal speed as the system cools. The problem was that one-body dissipation, the favorite theoretical concept, is essentially independent of T. Nevertheless, the first systematic excitation function

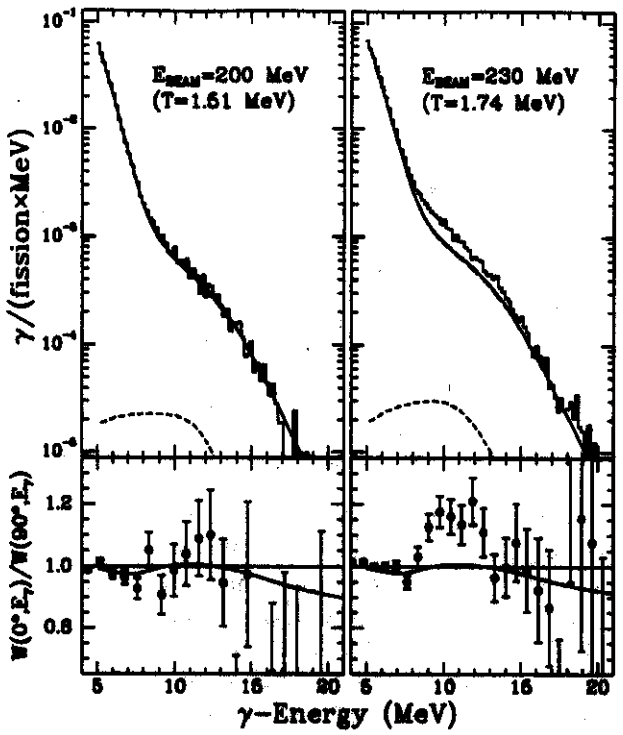

Figure 15: Comparison of the γ-ray spectra and angular correlations of the reaction $^{32}S + ^{208}Pb$ at 200 and 230 MeV. Fits are with the nondissipative statistical model. From Ref. 65.

studies of prefission neutron multiplicities (25) found a distinct onset of dissipation effects above a certain energy. This observation was confirmed in the reaction $^{19}F + ^{181}Ta \rightarrow ^{200}Pb$, in which nondissipative calculations could reproduce the data at an excitation energy of 69 MeV, whereas at 102 MeV these calculations underestimated the measured prefission GDR γ-ray yield (19). During the last few years, a large set of data using different probes (discussed in Section 6.1) demonstrated this onset. Here, we present new evidence for a rather rapid onset with the GDR clock.

The $^{32}S + ^{208}Pb \rightarrow ^{240}Cf$ reaction shown in Figure 15 for two bombarding energies directly demonstrates this dependence. Both data sets are compared with statistical model calculations without dissipation. In the right panel, at 230-MeV bombarding energy, the nondissipative statistical model (solid line) distinctly underestimates the γ-ray spectrum and the observed strong-correlation peak, which indicates emission from the compound system, is also not reproduced. This is, of course, as expected and led to the introduction of the strong dissipation discussed in

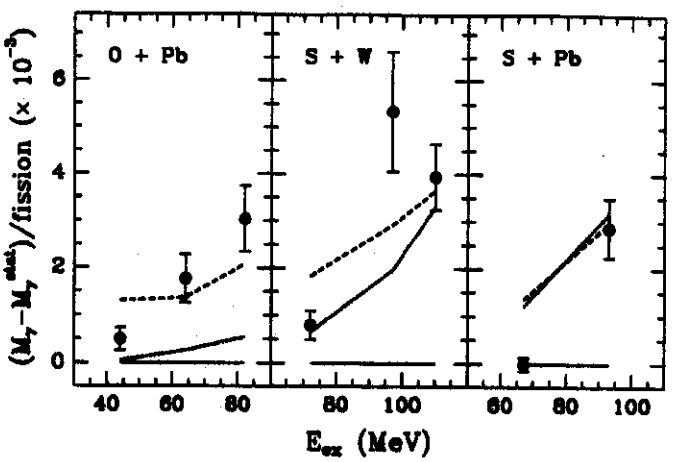

Figure 16: Excess prefission γ-ray multiplicity over the statistical model calculations as a function of energy for three different reactions. The curves are explained in the text. From Ref. 68.

the previous section. However, in the left panel, in which the bombarding energy is only 30 MeV lower, the data are explained perfectly without dissipation, and the angular correlation gives no evidence of γ rays from the compound system, ostensibly because it fissions too quickly to do so. Thus in this system dissipation apparently occurs only at bombarding energies $>$ 30 MeV. Because standard statistical-model calculations and dissipation calculations are in agreement (within 10%) for dissipation coefficients $\gamma < 0.15$ [the value derived for ground-state fission; ((31) and Section 1), the dissipation coefficient increases in the thorium system from < 0.15 to 10 over this narrow excitation energy range.

This same strong energy dependence was observed in all other GDR reactions studied to date. Figure 16 shows the enhancement of the γ-ray multiplicities over nondissipative CASCADE calculations as a function of excitation energy for three different reactions (65). Calculations that include dissipation only from the saddle-to-scission with $\gamma_o = 5$, or $\tau_{ssc} = 30 \times 10^{-21}$s, (dotted line) or including dissipation for both inside ($\gamma_i \sim 5$) and outside the saddle ($\gamma_o = 5$) (dashed line) cannot reproduce the strong excitation-energy dependence of the γ-ray excess.

This strong dependence of the dissipation on energy or temperature is probably the most interesting result to emerge from the recent experiments of nuclear dissipation because it challenges the historical understanding of dissipation in nuclear matter at low temperature. This dependence is discussed in more detail in Section 7.

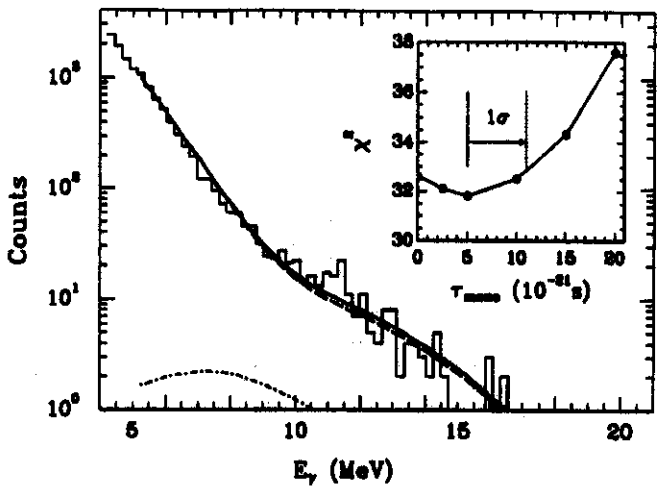

Figure 17: γ-ray spectrum following the reaction ^{58}Ni + ^{165}Ho at a bombarding energy of 368 MeV. The total calculated γ-ray spectrum (solid line) is dominated by the fission fragment contributions (dashed line) and γ rays from the intermediate system (dotted/dashed line) are almost negligible. From Ref. 68.

5.4 Time Scale of Quasifission

It is important to test the GDR clock against other dynamical processes whose time scales are known from completely different techniques. Two such reactions are deep inelastic scattering and quasifission, which have been performed with reassuring results (68). We discuss here only the case of quasifission, introduced in Section 4. The quasifission process dominates the total reaction cross section in rather symmetric reactions where large extra-extra-push effects are present. The extra-push model (51, 70, 71) predicts for the reaction ^{58}Ni + ^{165}Ho at a bombarding energy of 368 MeV that only 150 mb of a 550-mb capture cross section will fuse to the compound nucleus ^{233}Am and that 400 mb will form an intermediate system that reseparates after mass equilibration.

Figure 17 shows the γ-ray spectrum in coincidence with quasifission fragments. The γ rays emitted from the intermediate system can be treated similarly to the emission from the saddle-to-scission process, described in Section 4.2. The resultant total γ-ray spectrum (solid line) contains only very small contributions from the GDR decay of the intermediate system (dotted/dashed line). The contribution from the fission fragments alone (dashed line) is nearly sufficient to describe the data. A χ^2 fit results in a lifetime of the quasifission process of $\tau_{QF} = (5 \pm 5) \times 10^{-21}$ s. This result agrees with quasifission lifetimes of $2-8 \times 10^{-21}$ s observed in the reaction ^{238}U + ^{64}Ni (49, 52). A calculation using the dissipative col-

lision code HICOL (72), which includes full one-body dissipation, yields a quasifission lifetime of 12×10^{-21} s, which is averaged over the angular momentum population.

6. DISSIPATION EFFECTS IN OTHER CHANNELS

6.1 Neutron and Charged-Particle Evaporation

When it became possible to separate kinematically neutrons emitted by the compound nucleus from those emitted by fission fragments one could also extract fission lifetimes from prefission neutron multiplicities. Early experiments measured prescission neutron multiplicities that, above a certain energy, were larger than predicted by the statistical model. Since then a wealth of neutron data over a wide mass range and at temperatures up to 3 MeV have been collected. Hilscher and Rossner summarized these data as well as multiplicity measurements of charged particles (5). The higher prescission particle multiplicities have been interpreted as evidence of dissipation in the fission process. We restrict ourselves here to comparing the different analysis methods and assessing the consistency of the results between neutron and γ-ray data.

Only for a few systems have both the prefission γ rays and the prefission neutron multiplicities been measured (26, 73, 74) and only in one case have both observables been measured by the same group (75). However, the modified statistical models used in the analysis of the prefission γ-ray spectra also yield prefission neutron multiplicities without any additional free parameter.

Figure 18 shows the prescission neutron multiplicities observed in the reaction $^{16}O + {}^{208}Pb$ as a function of excitation energy (73, 74). Calculated neutron multiplicities from CASCADE with the same large dissipation constant $\gamma = 10$ that fit the prescission γ-ray spectra are also in closest agreement with the neutron data. Lower values of $\gamma = 0.1$, $\gamma = 1$ and $\gamma = 5$ clearly underestimate the measured neutron multiplicities. Conversely, the analysis methods applied to the neutron measurements to predict the γ-ray data is not as easy: Either these methods typically do not include the γ-ray decay or, in the case of Monte Carlo codes, the extraction of the γ-ray decay is impractical because the γ-ray decay branch is only $\sim$0.1% of the neutron channel.

Figure 19 depicts the time scales derived from prescission neutron multiplicity measurements for compound nuclei between Z = 85 and Z = 91 as a function of excitation energy (73). At first sight, the compound nucleus lifetime for ^{224}Th at E_{ex} = 64 MeV, extracted from the GDR

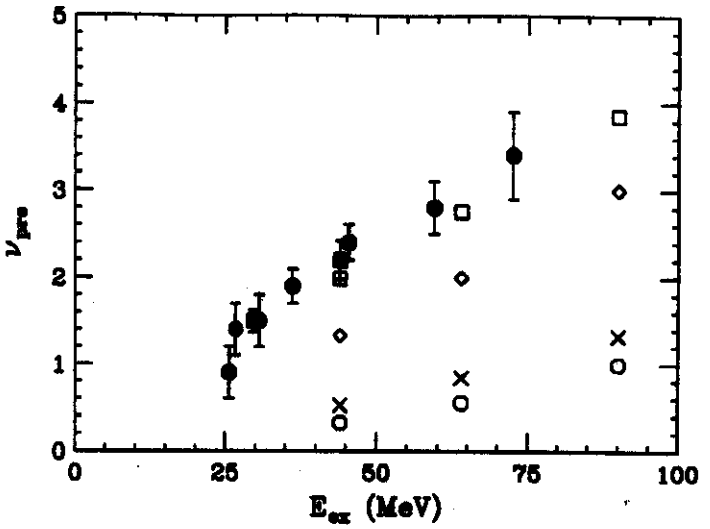

Figure 18: Experimental prescission neutron multiplicities from Ref. 73 (■) and Ref. 74 (•) for the reaction $^{16}O + ^{208}Pb$ compared with statistical model calculations with $\gamma = 0.1$ (o), $\gamma = 1$ (×), $\gamma = 5$ (◇), and $\gamma = 10$ (□) (26).

measurements, appears considerably larger than the lifetimes deduced from the neutron analysis: $\tau_f = 6.4 \times 10^{-19}$ s (26). This difference, however, is largely due to differences among the analysis methods and the varying definitions of the fission time scales.

First, the extracted lifetime in the statistical model depends on the level density parameter. The neutron data were analyzed using A/10 (73), whereas the analysis of the γ-ray data used A/8.8. A change from A/10 to A/8 increases the extracted fission time by a factor of 2, which moves toward the γ-ray data. Second, the lifetimes in the γ-ray analyses are given by the sum of the equilibration lifetime and the saddle-to-scission time. The equilibration lifetime is deduced directly from the average fission decay width (Γ_{Kra}) in the statistical model, which takes the fission delay time τ_D into account and is thus a lifetime in the true statistical sense. The saddle-to-scission time is a fixed time interval and is added to the equilibrium lifetime to yield the total fission time. The delay time analyses of the prefission neutron multiplicity measurements typically use a different approach. Fission is inhibited completely at the beginning of the decay and then turned on to the full Bohr-Wheeler (not Kramers) decay width after the fission delay time. The total time is $\tau_f = \tau_{delay} + \tau_{ssc}$. Thus the subsequent fission lifetime of the statistical calculation is not included, which results in smaller values of the fission time. Finally, the use of a step function instead of an exponential (76) produces for the same fission width a time scale a factor of four

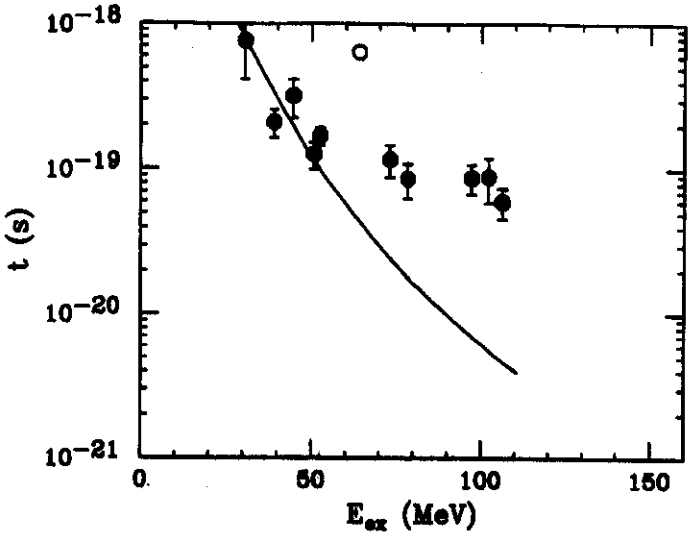

Figure 19: Fission lifetimes extracted from prescission neutron multiplicities for compound nuclei between Z = 85 and Z = 91 (•) and from γ-ray measurements of ^{232}Th (o) plotted vs initial excitation energy. The solid line indicates fission lifetimes from nondissipative statistical model calculations. Adapted from Ref. 73.

shorter than the exponential. Using a larger fission width by excluding the Kramers factor tends to compensate for this effect.

One can also compare the surprising onset of dissipation effects with excitation deduced from the GDR clock with the results from different methods. These effects were first observed in the prefission neutron multiplicity measurements (25), which when compared with statistical model calculations showed deviations only above a certain excitation energy (see Figure 19). In addition to the heavy-ion-induced prefission neutron data (5, 25, 46, 47, 73), prefission charged particles (77) and prefission neutron measurements following the proton-induced fission of uranium (78) all exhibit an onset of dissipation. In a very elegant experiment Eckert et al dedeuced the onset of dissipation from the sequential fission of ^{232}Th following peripheral collisions with 30 MeV/A ^{40}Ar (79). This experiment sampled the entire excitation energy range at once.

Figure 20 gives a compilation of the onset of dissipation derived from all of these different data sets (80). The threshold energy (threshold temperature) is defined as the excitation energy at which the statistical models without dissipation begin to fail. In the figure, the ratio of threshold temperature to average fission-barrier energy is plotted as a function of mass for the particle multiplicity data, the peripheral collision data, and the onset data derived from the γ-ray measurements. With the exception of two γ-ray data points dissipation begins tp dominate when the

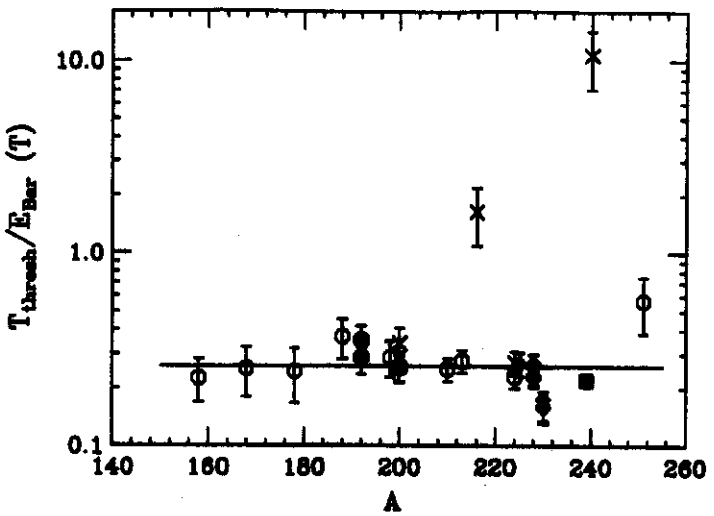

Figure 20: Ratio of the threshold temperature to the average fission barrier as a function of mass for the heavy-ion neutron (o), proton-induced neutron (□), charged particle- (•) and γ-ray (×) multiplicities and for the peripheral collision data (◇). From Ref. 80.

temperature reaches ~20% of the average fission barrier.

The prefission charged-particle measurements are somewhat controversial. Ikezoe et al found that prefission proton and α multiplicities of reactions thoroughly studied with prefission neutron measurements could be fitted with standard statistical model parameters (81). This observation conflicts with the neutron data. Because the charged-particle data depend on the emission threshold as an additional adjustable parameter, they are not as reliable as the neutron data.

6.2 Fusion-Evaporation Cross Section

A large fraction of prefission γ-ray data was taken at high excitation energies in very fissile systems in which essentially the entire fusion cross section fissions. However, even a small cross section leading to evaporation residues is an important constraint on the parameters of the statistical calculations. Dissipation inside the saddle reduces the overall fission probability, as mentioned in Section 5.1, and thus increases the evaporation cross section unless other parameters are adjusted. To explain a very small evaporation cross section, the fission barrier was reduced to as little as 70% of the Sierk barrier (32) in the early analyses of γ-ray data. However, even if dissipation has a strong temperature dependence, it alters the fission probability only beyond a certain temperature. Thus, once the compound nucleus cools down, the normal (Bohr-Wheeler) fis-

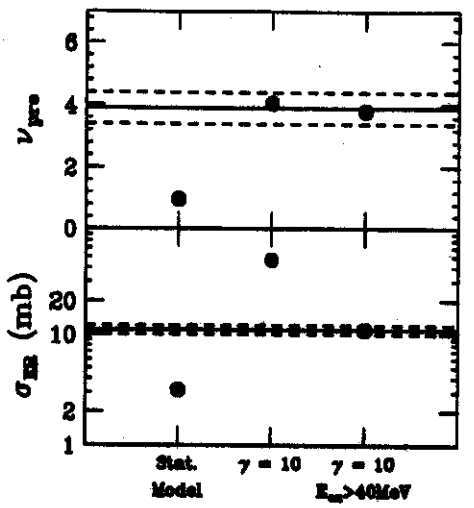

Figure 21: Comparison of three different statistical model calculations for the reaction $^{16}O + ^{208}Pb$ at $E_{lab} = 140$ MeV with measured evaporation residue cross section (bottom) (82) and prefission neutron multiplicity (top). The solid and dashed lines correspond to the data and error margins, respectively.

sion probability is regained in the final cooling steps, and the effect on the evaporation cross section is reduced. Unfortunately, fusion-evaporation cross sections have been measured for only a few systems for which prefission particle/γ-ray multiplicity data exist. To determine accurately the evaporation cross section in actinides and heavier nuclei is tricky; recent measurements yielded substantially larger cross sections than did previous experiments

An instructive example are the recent results of the reaction $^{16}O + ^{208}Pb$, which wasremeasured carefully and extended from the threshold at 80 MeV up to 140 MeV (82). At 140 MeV, the cross section is surprisingly large; $\sigma_{ER} = 11 \pm 1$ mb. For Figure 21 we chose this data point to demonstrate how this value constrains the statistical model calculations for the γ-ray and neutron multiplicities. The value for the prefission neutron multiplicity (3.9 ± 0.5) was interpolated between the data shown in Figure 18 and a measurement of $\nu_{pre} = 6.9 \pm 0.3$ at $E_{ex} = 187$ MeV (83).

Standard statistical-model calculations clearly underestimate the evaporation-residue cross section, the prefission neutron multiplicity and, of course, the prefission γ-ray spectrum. A dissipation constant $\gamma = 10$ is necessary to describe the pre-fission γ-ray multiplicity (see Figure 11). With this value of γ, the statistical models reproduce the prefission neutron multiplicities, but they significantly overestimate the evaporation residue cross section. As discussed above, including the energy thresh-

old for the dissipation, which lies between 30 and 40 MeV (68, 80) for ^{232}Th, gives agreement with all three data sets. Thus the description of γ-ray spectra by the statistical model with an energy-dependent dissipation is consistent with all available experiments without any arbitrary adjustments of statistical-model parameters.

6.3 Formation Time Scales

All simulations discussed thus far assumed that a fully equilibrated compound nucleus is formed at a time $t = 0$, which is the starting point of the calculations. The time of formation is taken to be negligible. However, this assumption is not always valid. In peripheral collisions of (almost) symmetric heavy-ion reactions, dissipation reduces the fusion cross section (extra-extra push effect) (51, 70, 71). Calculations using full one-body dissipation demonstrate that the fusion process is quite slow in this case, and the compound nucleus formation time may be comparable to particle evaporation times of the compound nucleus (72).

Indeed, this effect was observed in the fusion evaporation reaction of ^{64}Ni + ^{100}Mo (84). In this system (which does not involve fission), the high energy γ-ray spectrum could not be described with the standard statistical model but required inclusion of γ-ray and particle emission during the formation time. The modifications to the statistical model are essentially identical to those that describe emission during the saddle-to-scission motion, except that they precede the equilibrium decay.

Thus for rather symmetric reactions leading to compound nucleus formation with subsequent fission, one must consider the γ-ray contribution from the formation time. However, distinguishing those contributions from the saddle-to-scission decay, is virtually impossible because it is essentially the inverse process. For quasifission reactions, no compound nucleus is formed, and a $t = 0$ therefore does not exist. Thus, the quasifission time scale inherently includes the formation time and represents the total time from approach to reseparation of the intermediate system.

Along related lines, differences in formation times are predicted if the same compound nucleus is formed in reactions of different projectile-target mass asymmetry α, which are smaller or larger than the Businaro-Gallone critical asymmetry value α_{BG} (85). Reactions with $\alpha > \alpha_{BG}$ form the compound nucleus faster than those with $\alpha < \alpha_{BG}$. This effect has also been observed. Prescission neutron emission in the more symmetric reaction ^{16}O + ^{232}Th is larger than in the reaction ^{11}B + ^{237}Np, which results in fission times $\tau_f = 50 \pm 5 \times 10^{-21}$ s and $\tau_f = 35 \pm 5 \times 10^{-21}$ s, respectively (86). Both reactions lead to ^{248}Cf. The difference of

$10 - 15 \times 10^{-21}$ s was attributed to the formation time of the compound nucleus. However, this time is significantly longer than the formation times calculated with the dissipative collision code HICOL (72) which assumes full one-body dissipation. It predicts a difference of 3×10^{-21} s between the formation times of the ^{11}B- and ^{16}O-induced reactions. This prediction of small differences is supported by a GDR γ-ray measurement in the mass region A $\sim$ 140 (87). This experiment studied the reactions ^{16}O + ^{126}Te and ^{22}Ne + ^{120}Sn which lead to the same compound nucleus ^{142}Nd at E_{ex} = 150 MeV. These reactions have asymmetries larger and smaller than α_{BG}, respectively. The γ-ray spectra did not show any differences that could be attributed to differences in the formation times. This result is also in agreement with HICOL calculations, which predicted $\Delta t = 1 \times 10^{-21}$ s. The calculated formation times for the systems discussed here are significantly shorter than the extracted fission lifetimes and thus should not be important for the topics of this review.

7. DISCUSSION AND CONCLUSION

Here we summarize the results of the γ-ray multiplicity studies as. The GDR clock, in agreement with the neutron clock and other techniques, shows clear and systematic evidence for strong dissipation in fission mass flow. The dissipation sets in rather rapidly at nuclear excitation energies above ~40 MeV, depending somewhat on the reaction and mass of the compound system. These excitation energies correspond to compound nuclear temperatures of T $\sim$ 1.3 MeV. In addition, the GDR clock demonstrates that, above this temperature, strong dissipation is present inside the barrier, with a dissipation constant γ_i = 10 ($\pm$3), as well as outside the saddle, with γ_o = 5 ($\pm$ 1). Thus the mass motion is strongly overdamped everywhere.

Are these observations consistent with the present theoretical understanding of nuclear dissipation? We refer the reader to Ref. 5 for an overview of this subject and concentrate here on a qualitative discussion of some recent developments. Before making any quantitative comparison between the extracted dissipation constant and the theoretical predictions, however, one must consider the assumptions made in the analysis of the data: One classical (Thomas-Reiche-Kuhn) electric-dipole sum-rule strength has been assumed for the GDR, and in the deformed nucleus this strength was distributed according to the ratio of degenerate deformation axes. At the barrier, $\hbar\omega \sim T$, and the frequencies of the potential minimum and of the barrier have been set equal: $\omega_1 \approx \omega_2$.

Although $\omega = 1 \times 10^{21} s^{-1}$ is a convenient scaling value for the collective frequency to relate $\gamma_{i,o}$ to the collision frequency β, this translation can be performed more carefully in a quantitative comparison.

Because of the long mean free path of nucleons in cold nuclear matter, nuclear dissipation has been explained mostly in terms of one-body dissipation (88) in which nucleons interact only with the (moving) nuclear boundary. One-body dissipation also has been applied to many other dissipative reaction processes, such as deep inelastic scattering and quasifission (72), with great success. In a fissioning system, one-body dissipation can be related to the randomization of classical single-particle orbits in the mean field boundary (89). This process is effective only for large-order deformations; thus the full strength of one-body dissipation is expected only during the strongly deformed stages of the fission process. Here it is not surprising that one-body dissipation explains the long saddle-to-scission times as well as the fission-fragment kinetic energies (90). The role of one-body dissipation was confirmed recently by extensive calculations using the Langevin equation to describe the evolution of the collective parameters coupled to a statistical model for particle and γ-ray emission (91- 93). These calculations yield the correct neutron and γ-ray multiplicities when parameters consistent with the experimental analysis are used. This detailed dynamical description made it possible to confirm that one-body dissipation is ineffective in compact shapes, i.e. inside the saddle.

On general grounds, one-body dissipation has at most a $T^{1/2}$ temperature dependence and is prima facie unable to explain the observed threshold for strong dissipation. However, the one-body dissipation model assumes that equilibrium is established among all nucleons in the nuclear interior, between wall bounces. This condition may not be fulfilled below a minimum temperature. The onset of chaoticity in nuclei has been considered in terms of several nuclear structure models (e.g. see Ref. 94) and may be different for strongly rotating nuclei (95, 96). For instance, Hoffman predicted that, during the collective motion, shell effects vanish at $T \sim 2$ MeV (97).

Because the saddle shapes of the heavy nuclei discussed here are quite compact, only strong two-body dissipation appears able to reproduce the observed strong dissipation inside the saddle. Some calculations using the (two-dimensional) Langevin equation have included an adjustable two-body viscosity (67). A viscosity of 0.2 tera poise (TP) ($\sim$10 times the commonly accepted value) is required to fit the neutron multiplicities, but this value underestimates the fragment kinetic energies. However, a mixture of one- and two-body dissipation for the inside

and the outside might eliminate this discrepancy because the kinetic energies reflect the dissipative losses outside the saddle. Calculations using a one-dimensional Langevin equation (98) with a microscopically introduced two-body viscosity give a very large dissipation, with a collision frequency $\beta = 77 \times 10^{21}$ s^{-1} at T = 3 MeV, dropping to $5 \times 10^{21} s^{-1}$ at T = 4 MeV, in ^{248}Cf.

Linear-response theory predicts that two-body dissipation rises rapidly from T $\sim$ 1 MeV to T $\sim$ 2 MeV. This could explain the observed energy threshold of γ_i (99) which, until recently, was much too weak.

The temperature dependence of two-body dissipation is a much-debated subject, and predicted dependences range from powers larger than T^2 to T^{-2}. One is tempted to seek guidance from the Fermi liquid theory (100) by considering the build up of the fission flux inside the saddle as a pressure wave, i.e. coherent flow of nucleons, in the nuclear interior. The mean free path and thus the local relaxation time τ_r of a pressure wave with frequency ω varies as $\tau_r \sim 1/T^2$. At a sufficiently high temperature, when $\omega\tau_r << 1$ the wave achieves local equilibrium, and its amplitude is attenuated proportional to $1/T^2$ (first sound). However, at low temperatures, $\omega\tau_r >> 1$, local equilibrium is not achieved, and the wave is attenuated proportional to T^2 (zero sound). Thus two-body bulk dissipation increases first as T^2 up to a critical temperature, then decreases as $1/T^2$. This change is observed in transport measurements of liquid ^{3}He (100, 101). The temperature at which the turnover occurs in nuclear matter has not been well established.

Finally, the prediction from linear-response theory that two-body dissipation is very weak may be true only for nonrotating nuclei. Pomorski & Hofman recently proposed that this dissipation could be much larger in nuclei at high rotational frequency (102), which includes all experimental cases cited here. For an average value L = 50$\hbar$, they compute a friction constant β along the symmetry axis as large as $\beta = 48 \times 10^{-21}$ s^{-1}. This value corresponds to $\gamma = \beta/2\omega \approx 24$ at T = 1 MeV, a dissipation even larger than what is observed. From 1 to 2 MeV, the dissipation increases by another 50% but then saturates between 2 and 3 MeV. This behaviour then would explain all available data.

It is therefore of great interest to investigate the energy regime over which dissipation increases rapidly in more detail and to extend the measurements to much higher temperatures to verify the predicted rise and saturation and perhaps even observe a decrease as a function of T. It would also be useful to further separate out dissipation in the interior by detecting γ rays in coincidence with evaporation residues. This coincidence requirement would eliminate the γ-ray background from fission

fragment and might make the upshifted GDR component of the deformed compound system apparent in the correlation. It would also allow extension of these studies to even heavier systems. However, for experimental and reaction dynamical reasons, such measurements will not be easy to perform.

Finally, one could question why the large dissipation in the collective mass flow does not appear to affect the vibrational frequency of the GDR itself. The answer lies in the fact that nuclear matter has elastoplastic properties (103), as Rhein recently also indicated by experiment (104). Thus the medium responds elastically to the fast GDR vibration but plastically to the slow fission motion.

ACKNOWLEDGMENT

This work was supported in part by the US National Science Foundation. The authors wish to thank DJ Hofman for his many contributions to this research and for his help in preparing many of the figures.

Literature Cited

1. Morrissey DJ, Benenson W, Friedman WA, *Annu. Rev. Nucl. Part. Sci.* 44, this volume (1994), and references therein
2. Nix JR, *Nucl. Phys.* A130:241-92 (1969)
3. Vandenbosch R, Huizenga JR, *Nuclear Fission*, New York: Academic (1973)
4. Davies KTR, Sierk AJ, Nix JR, *Phys. Rev.* C13:2385-403 (1976)
5. Hilscher D, Rossner H, *Ann. Phys. Fr.* 17:471-552 (1992)
6. Snover KA, *Annu. Rev. Nucl. Part. Sci.* 36:545-603 (1986)
7. Gavron A, et al. *Phys. Rev. Lett.* 47: 1255-58 (1981), 48:835-36(E) (1982)
8. Holub E, et al. *Phys. Rev.* C28:252-70 (1983)
9. Hinde DJ, et al. *Phys. Rev. Lett.* 52:986-89 (1984), 53:2275-76 (1984)
10. Thoennessen M, et al. *Phys. Rev. Lett.* 59:2860-63 (1987)
11. Stokstad RG, *Treatise on Heavy Ion Science*, ed. DA Bromley, 3:83-197, New York: Plenum (1985)
12. Chakrabarty DR, et al. *Phys. Rev.* C36:1886-95 (1987)
13. Gaardhøje JJ, *Annu. Rev. Nucl. Part. Sci.* 42:483-536 (1992)
14. Kicińska-Habior M, et al. *Phys. Rev.* C45:569-75 (1992)
15. Gundlach JH, et al. *Phys. Rev. Lett.* 65:2523-26 (1990)
16. Beil H, et al. *Nucl. Phys.* A227:427-49 (1974)
17. Chbihi A, et al. *Phys. Rev.* C43:666-77 (1991)
18. Shlomo S, Natowitz JB, *Phys. Rev.* C44:2878-80 (1991)
19. Butsch R, et al. *Phys. Rev.* C41: 1530-44 (1990)
20. Thoennessen M, *Giant dipole resonance in highly excited Pb and Th nuclei* Ph.D. thesis, State University of New York at Stony Brook, unpublished (1988)
21. Grangé P, Weidenmüller HA, *Phys. Lett.* 96B:26-30 (1980)
22. Grangé P, Jun-Qing Li, Weidenmüller HA, *Phys. Rev.* C27:2063-77 (1983)
23. Weidenmüller HA, *Progress in Particle and Nuclear Physics*, 3:49-126, Oxford: Pergamon (1980)
24. Grangé P, et al. *Phys. Rev.* C34:209-17 (1986)

25. Hinde DJ, et al. *Nucl. Phys.* A452: 550-72 (1986)
26. Butsch R, et al. *Phys. Rev.* C44: 1515-27 (1991)
27. Bhatt KH, Grange P, Hiller B, *Phys. Rev.* C33:954-68 (1986)
28. Bohr N, Wheeler JA, *Phys. Rev.* 56: 426-50 (1939)
29. Kramers HA, *Physica* 7:284-304 (1940)
30. Hofmann H, Nix JR, *Phys. Lett.* 122B:117-20 (1983)
31. Dagdeviren NR, Weidenmüller HA, *Phys. Lett.* 186B:267-71 (1987)
32. Diószegi I, et al. *Phys. Rev.* C46:627-36 (1992)
33. Laval M, et al. *Nucl. Instrum. Methods* 206:169-76 (1983)
34. Kubota S, et al. *Nucl. Instrum. and Methods* 242:291-94 (1986)
35. Sen S, et al. *Nucl. Instrum. and Methods* 264:407-09 (1988)
36. Sobotka LG, et al. *Phys. Rev.* C44: R2257-61 (1991)
37. Ford RL, Nelson WR, SLAC Rep. 210 (1978) (unpublished)
38. Brun R, et al. *GEANT3 Users Guide*, Data Handling Div. DD/EE/84-1, CERN (1986)
39. Pühlhofer F, *Nucl. Phys.* A280:267-84 (1977)
40. Gavron A, *Phys. Rev.* C21:230-36 (1980)
41. Blann M, Komoto TT, *Phys. Rev.* C26:472-85 (1982)
42. Reisdorf W, *Nucl. Phys.* A444:154-88 (1985)
43. Sierk AJ, *Phys. Rev.* C33:2039-53 (1986)
44. Newton JO, Popescu DG, Leigh JR, *Phys. Rev.* C42:1772-74 (1990)
45. Grangé P, *Nucl. Phys.* A428:37c-62c (1984)
46. Gavron A, et al. *Phys. Rev.* C35:579-90 (1987)
47. Newton JO, et al. *Nucl. Phys.* A483: 126-52 (1988)
48. Hassani S, Grangé P, *Phys. Lett.* 137B: 281-86 (1984)
49. Shen WQ, et al. *Phys. Rev.* C36:115-42 (1987)
50. Keller JG, et al. *Phys. Rev.* C36: 1364-74 (1987)
51. Bjørnholm S, Swiatecki WJ, *Nucl. Phys.* A391:471-504 (1982)
52. Tōke J, et al. *Nucl. Phys.* A440:327-65 (1985)
53. Green AES, *Nuclear Physics*, New York: McGraw Hill (1955)
54. Viola VE, Kwiatkowski K, Walker M, *Phys. Rev.* C31:1550-52 (1985)
55. Schmitt RP, Mouchaty G, Haenni DR, *Nucl. Phys.* A427:614-38 (1984)
56. Dietrich FS, et al. *Phys. Rev.* C10: 795-802 (1974)
57. Glässel P, et al. *Nucl. Phys.* A502: 315c-24c (1989)
58. Kasagi J, et al. *J. Phys. Soc. Jpn.* 58(Suppl.):620-25 (1989)
59. Luke SJ, Gossett CA, Vandenbosch R, *Phys. Rev.* C44:1548-54 (1991)
60. van der Ploeg H, et al. *Phys. Rev. Lett.* 68:3145-47 (1992), 69:1148(E) (1993)
61. van der Ploeg H, et al. *Nucl. Phys.* A569:83c-92c (1994)
62. Hofman DJ, et al. *Phys. Rev.* C47: 1103-07 (1993)
63. Thoennessen M, et al. *Phys. Lett.* B282:288-92 (1992)
64. Hasse RW, Schuck P, *Phys. Lett.* B179:313-16 (1986)
65. Hofman DJ, et al. *Phys. Rev. Lett.* 72:470-73 (1994)
66. Nix JR, Sierk AJ, *Proc. Adriat. Int. Conf. Nucl. Phys.: Front. Heavy-Ion Phys. 6th, Dubrovnik, Yugoslavia, 1987*, ed. N Cindro, R Caplar, W Greiner, pp. 333-40, Singapore: World Scientific (1990)
67. Wada T, Carjan N, Abe Y, *Nucl. Phys.* A538:283c-89c (1992), *Phys. Rev. Lett.* 70:3538-41 (1993)
68. Paul P, *Nucl. Phys.* A569:73c-82c (1994)
69. Gaardhøje JJ, Maj A, *Nucl. Phys.* A520:575c-94c (1990).
70. Swiatecki WJ, *Physica Scr.* 24:113-22 (1981)
71. Swiatecki WJ, *Nucl. Phys.* A376: 275-91 (1982)
72. Feldmeier H, *Rep. Prog. Phys.* 50: 915-94 (1987)

73. Hinde DJ, Hilscher D, Rossner H, *Nucl. Phys.* A502:497c-514c (1989)
74. Rossner H, et al. *Phys. Rev.* C45: 719-25 (1992)
75. Schmitt RP, et al. *Int. Workshop Dyn. Asp. Nucl. Fission, Smolenice, Czechoslovakia, Cycl. Inst. Rep. #91-13*, Texas A&M University, unpublished (1991)
76. Back BB, *Proc 9th Winter Workshop Nucl. Dyn.*, ed. B Back, W Bauer, J Harris, pp. 15-21, Singapore: World Scientific (1993)
77. Lestone JP, et al. *Phys. Rev. Lett.* 67:1078-81 (1991)
78. Strecker M, et al. *Phys. Rev.* C41: 2172-87 (1990)
79. Eckert E-M, et al. *Phys. Rev. Lett.* 64:2483-86 (1990)
80. Thoennessen M, Bertsch GF, *Phys. Rev. Lett.* 71:4303-06 (1993)
81. Ikezoe H, et al. *Nucl. Phys.* A538: 299c-305c (1992)
82. Brinkmann K-T, et al. *Phys. Rev.* C50 In press (1994)
83. Hinde DJ, et al. *Phys. Rev.* C45: 1229-59 (1992)
84. Thoennessen M, et al. *Phys. Rev. Lett.* 70:4055-58 (1993)
85. Businaro UL, Gallone S, *Nuovo Cimento* 5:315 (1957)
86. Saxena A, et al. *Phys. Rev.* C49:932-40 (1994)
87. Choudhury RK, et al. *Nucl. Phys.* 569:93c-100c (1994)
88. Blocki J, et al. *Ann. Phys.* 113:330-86 (1978)
89. Swiatecki WJ, *Nucl. Phys.* A488: 375c-94c (1988)
90. Carjan N, Sierk AJ, Nix JR, *Nucl. Phys.* A452:381-97 (1986)
91. Gontchar, II, Fröbrich P, *Nucl. Phys.* A551:495-507 (1993)
92. Fröbrich P, Gontchar II, Mavlitov ND, *Nucl. Phys.* A556:281-306 (1993)
93. Fröbrich P, Gontchar II, *Nucl. Phys.* A563:326-48 (1993)
94. Whelan N, Alhassid Y, *Nucl. Phys.* A556:42-66 (1993)
95. Aberg S, *Phys. Rev. Lett.* 64, 3119-22 (1990)
96. Alhassid Y, *Proceedings in Physics*, 58:41-91, Berlin: Springer (1991)
97. Hofmann H, *Int. Conf. Nucl. Struct. Nucl. React. Low Intermed. Energ.*, Dubna: Dubna Press (1992)
98. Boilley D, et al. *Nucl. Phys.* A556: 67-87 (1993)
99. Strumberger E, Dietrich K, Pomorski K, *Nucl. Phys.* A502:523c-30c (1989)
100. Baym G, Pethick Ch, *Landau Fermi-Liquid Theory* , p.53, New York: Wiley (1991)
101. Abel WR, Anderson AC, Wheatley JC, *Phys. Rev. Lett.* 17:74-78 (1966)
102. Pomorski K, Hofman H, *Phys. Lett.* B263:164-68 (1991)
103. Bertsch, GF, *Sci. Am.* 248,Nr.5:62-73 (1983), Nöremberg W, *Heavy Ion Reaction Theory*, ed WQ Shen, JY Li, LX Ge, pp 1-36, Singapore: World Scientific (1989)
104. Rhein M, et al. *Phys. Rev. Lett.* 69:1340-43 (1992), *Phys. Rev.* C49: 250-65 (1994)